

# Lithium as a probe of stellar and galactic physics

Corinne Charbonnel<sup>1,2</sup> and Nikos Prantzos<sup>3</sup>

<sup>1</sup>Department of Astronomy, University of Geneva, Chemin Pégasi 51, 1290 Versoix, Switzerland; email: corinne.charbonnel@unige.ch

<sup>2</sup>IRAP, UMR 5277 CNRS and Université de Toulouse, 14 Av. E.Belin, 31400 Toulouse, France

<sup>3</sup>Institut d'Astrophysique de Paris, UMR7095 CNRS, Sorbonne Université, 98bis Bd. Arago, 75104 Paris, France

XXXX. XXX. XXX. XXX. YYYY. AA:1–48

[https://doi.org/10.1146/\(\(please add article doi\)\)](https://doi.org/10.1146/((please add article doi)))

Copyright © YYYY by the author(s).  
All rights reserved

## Keywords

Stars and the Sun: abundances, interiors, physical processes, angular momentum; nucleosynthesis; the Galaxy: chemical evolution, radial migration

## Abstract

Lithium plays a unique role in astrophysics, as it is a powerful diagnostic for the physics and evolution of low-mass stars, Galactic archaeology, and cosmology. We review the Li observations in stars at different phases of their evolution, the strengths and the limitations of the current theoretical stellar models to explain the Li abundance data, our understanding of the Li sources and of the evolution of Li throughout the Galactic history. Key takeaways from the current state of the research in the field are:

- Stellar evolution models accounting for fundamental transport processes of chemical species and angular momentum hold the promise of providing a common “stellar Li depletion” explanation to the Li abundance patterns observed in all Galactic stellar populations, including the “dip” and the “plateau(s)”.
- Novae are most probably the main source of Li in the Galaxy, on observational (but not yet theoretically established) grounds.
- Radial migration of stars in the Galactic disk holds the key to understand many aspects of the Li evolution in the Milky Way.

## Contents

1. INTRODUCTION .....	2
2. LITHIUM AS A PROBE OF STELLAR PHYSICS .....	3
2.1. The historical constraint of lithium depletion on stellar modelling .....	3
2.2. Observational evidence of Li depletion in low-mass dwarf stars.....	5
2.3. Observational evidence of Li dilution and depletion in evolved low-mass stars, and the case of Li-rich red giants.....	9
3. HOW DO STARS DEPLET LITHIUM.....	12
3.1. Atomic diffusion and competing processes .....	12
3.2. Type I rotating models.....	14
3.3. Type II rotating models with magnetic instabilities .....	16
3.4. Type II rotating models with magneto-inertial gravity waves .....	17
3.5. Lithium depletion along the red giant branch .....	20
4. PRODUCTION OF LITHIUM IN ASTROPHYSICAL ENVIRONMENTS.....	21
4.1. Spallation reactions in cosmic rays .....	23
4.2. Primordial nucleosynthesis .....	24
4.3. Hot Bottom Burning in Asymptotic Giant Branch stars .....	25
4.4. Explosive H-burning in novae .....	26
4.5. $\nu$ induced nucleosynthesis in core-collapse supernovae .....	27
5. LITHIUM AS A PROBE OF THE CHEMICAL AND DYNAMICAL EVOLUTION OF THE GALAXY ..	28
5.1. The solar vicinity and the main Li source .....	28
5.2. Evolution of Li in the Milky Way thin disk .....	30
5.3. The evolution of Li in the thick disk and the bulge .....	33
5.4. The evolution of the ${}^6\text{Li}/{}^7\text{Li}$ ratio .....	34

## 1. INTRODUCTION

Lithium (Li), the third lightest element in the periodic table, holds a unique position in astrophysics as it probes the properties of the outer layers of stars, the baryonic density of the Universe, and the chemical evolution of the Galaxy. Despite the relative simplicity of its atomic structure, the abundance and distribution of Li in stellar environments remain enigmatic and continue to challenge our understanding of stellar structure, nucleosynthesis, and galactic chemical evolution. Li is the only element for which whole workshops or conferences are held (e.g. Paris 2012 or Rome 2019) and monographs are written (Martín 2023).

The  ${}^7\text{Li}$  (hereafter Li) abundance is now available for tens of thousands of low-mass stars in different areas of the colour-magnitude diagram, thanks to the many spectroscopic surveys (e.g. Gaia-ESO, GALAH, LAMOST) that are complementing the ESA Gaia mission to decipher the history of the Milky Way and asteroseismic surveys that probe the interior of stars (CoRoT, *Kepler*, K2, TESS, and the future PLATO).

Of all Li discoveries, the one of Spite & Spite (1982) had probably the deepest impact in the fields of stellar and galactic astronomy and cosmology. Old dwarf stars of the Galactic halo display remarkably constant Li abundances which seem independent of their metal content (unlike any other metal) and of their properties, such as effective temperature (unlike the younger stars of the Galactic disk). The original interpretation of this pattern as a relic of the primordial nucleosynthesis met with difficulties twenty years later, after

the analysis of observations of the Cosmic Microwave Background (CMB) with the WMAP satellite favoured a higher cosmic density than suggested by the “halo plateau” of Li. A similar Li plateau has been discovered in Galactic dwarf stars from accreted satellites, including Gaia-Enceladus (Molnar et al. 2020, Simpson et al. 2021), and three S2-Stream members (Aguado et al. 2021). A variety of solutions were explored, including non-standard primordial nucleosynthesis and/or cosmologies as well as exotic particle physics, but these proved unsuccessful (Fields et al. 2020, and references therein). Currently, the most likely answer appears to be the “stellar Li depletion solution”.

The two Li isotopes,  $^6\text{Li}$  and  $^7\text{Li}$ , are the two most fragile stable nuclides after deuterium (D) and  $^3\text{He}$ . It is this property of nuclear fragility that made Li such a powerful tool enabling astronomers to “see” below the surfaces of stars and to probe their subphotospheric layers, well before the era of helio- and asteroseismology. In the 1950ies, it was realized that the Li abundance in chondrites - meteoritic inclusions in some of the oldest objects in the solar system - is higher than the one of the solar photosphere by more than two orders of magnitude. The Sun has severely depleted its original Li content since its birth in a way that is not predicted by classical stellar models. Various features observed in the Li abundance patterns of field stars and open clusters (OC), like the “Li-dip”, also call for physical processes beyond the “standard” ones of convection and atomic diffusion. While the understanding of the processes that transport angular momentum and chemicals in stars is one of the hottest topic in stellar physics thanks to the wealth of asteroseismic data,  $^7\text{Li}$  remains a unique and sensitive constraint on evolution models for low-mass stars. As of today, no model “passes” all the Li tests, but recent theoretical and numerical developments hold the promise of a common “stellar Li depletion solution” to all the Li abundance patterns observed in the different Galactic stellar populations, including the dip and the plateau.

The production mechanism of Li - as well as of the other light elements Be, and B - was an enigma to the founders of stellar nucleosynthesis, who coined the name ‘x-process’ for it (Burbidge et al. 1957). It was progressively realized that the most abundant isotope of lithium,  $^7\text{Li}$ , is the only nuclide produced in three different astrophysical sites: in the hot early Universe by primordial nucleosynthesis, in Galactic cosmic rays through spallation and fusion reactions, and in stars by thermonuclear reactions. Because of its fragility, the production of Li in stars remained elusive for decades. Only in the past ten years or so novae emerged as a serious candidate for the stellar source, supported by observations but not yet by theory. In view of the uncertainties in the production and depletion mechanisms of Li, the evolution of its abundance in a galactic context remains poorly understood, much more so than for any other element. Those issues - and several others - are the topic of this review.

## 2. LITHIUM AS A PROBE OF STELLAR PHYSICS

### 2.1. The historical constraint of lithium depletion on stellar modelling

In his seminal paper, which established the energy sources of normal (main sequence or MS) stars Bethe (1939) evaluated the reaction rates of all light nuclei with protons in conditions pertaining to the solar interior. He concluded that, in view of their fragility “...all the nuclei between H and C, notably  $\text{H}_2$ ,  $\text{H}_3$ ,  $\text{Li}_6$ ,  $\text{Li}_7$ ,  $\text{Be}_9$ ,  $\text{B}_{10}$ ,  $\text{B}_{11}$ , can exist in the interior of stars only to the extent to which they are continuously reformed by nuclear reactions”. Indeed, those nuclei are *destroyed* through  $(\text{p},\gamma)$  or  $(\text{p},\alpha)$  reactions in hot stellar interiors on timescales shorter than the stellar lifetimes, as illustrated in Fig. 1 (left).

---

**Metal:** An element heavier than Helium. *Metallicity* in stellar astronomy is usually expressed as  $[\text{Fe}/\text{H}] = \log((\text{Fe}/\text{H})_*/(\text{Fe}/\text{H})_\odot)$

### Li destruction:

Nuclear burning of Li through nuclear reactions with protons

### Li depletion:

Decrease of Li in the stellar photosphere compare to the original abundance

**Li dilution:** Decrease of the Li abundance due to dilution with Li-free material during the dredge-up episodes

It was soon realised that the strong dependence of the destruction rates of those nuclei on temperature, in conjunction with their abundances, as observed in stellar photospheres, provides a powerful probe of the inner layers of stars.

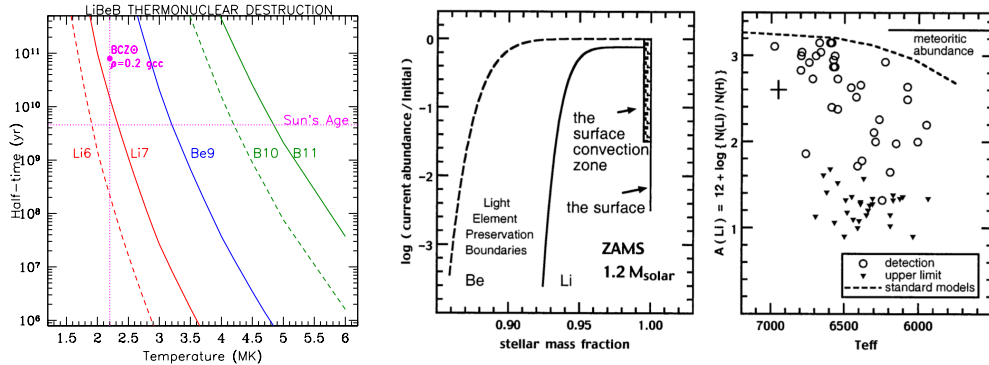


**Figure 1**

*Left* : Half-times (time of survival of half the original amount) of the light isotopes  ${}^6\text{Li}$ ,  ${}^7\text{Li}$ ,  ${}^9\text{Be}$ ,  ${}^{10}\text{B}$  and  ${}^{11}\text{B}$  as a function of temperature in an environment of solar composition and density  $\rho=1$   $\text{gr cm}^{-3}$ . Timescales for 2-body reactions are inversely proportional to  $\rho$ . The bottom of the convective zone of the Sun (BCZ $\odot$ ) has a density of  $\rho=0.2$   $\text{gr cm}^{-3}$ , implying a Li burning timescale larger than a Hubble time. *Middle*: Li and Be preservation zones in a classical stellar model of a  $1.2 M_\odot$ . The “step-like” abundance profile results from the temperature gradient in the external layers and the sensitivity to temperature of the proton captures on  ${}^7\text{Li}$  and  ${}^9\text{Be}$  (Fig. from Deliyannis et al. 2000). *Right*: Predictions of the classical theory, with only pre-main sequence Li depletion in cooler stars (Fig. from Deliyannis et al. 2000).

Greenstein & Richardson (1951) noticed that Li is depleted in the solar photosphere by a factor of  $\sim 100$  with respect to the Li meteoritic abundance and attributed that to its destruction through reactions with protons at temperatures  $T \sim 3 \times 10^6$  K (3 MK). They suggested that Li could be brought from the (much cooler) photosphere down to regions of such temperatures either by rotational or convective mixing. Subsequently, Greenstein & Tandberg Hanssen (1954) found that Be appears undepleted in the Sun. They suggested that combining these observations one may constrain the depth of the solar convective envelope, since Be destruction by proton capture happens at higher temperature (Fig. 1). The idea was quantitatively explored by Salpeter (1955) who used a purely radiative and chemically homogeneous solar model and determined that the bottom of the solar convective zone would lie at about half the solar radius, at temperatures between 2.6 and 3 MK. However, in the first solar models by Schwarzschild et al. (1957) accounting for convective equilibrium in the outer solar layers and chemical inhomogeneity caused by hydrogen burning in its interior, the base of the convective envelope reached a temperature of the order of 1 MK only. It was then proposed that the solar lithium depletion might have happened during its pre-main sequence contraction, when the base of its convective envelope was deeper and hotter. This was empirically proven insufficient by Herbig (1963) and Wallerstein et al. (1965)’s discovery of G-type main sequence stars with Li abundances similar to the meteoritic values in the young Pleiades OC, and of their slightly more Li-poor counterparts in

the slightly older Hyades. This was the first strong evidence for some mechanism(s) gently transporting Li from the bottom of the convective envelope of solar-type main sequence stars to the deeper radiative layers where it burns. Lithium was then definitively recognised as one of the key probes of the interior of low-mass stars, well before the emergence of helio- and asteroseismic constraints. Over the following sixty years, a plethora of observational surprises emerged (Sect.2.2 and 2.3), along with associated theoretical challenges to go beyond classical stellar modelling (Sect.3).

## 2.2. Observational evidence of Li depletion in low-mass dwarf stars

**2.2.1. The Sun and solar analogues.** A significant research effort has been dedicated to the reconstruction of the history of lithium depletion in the Sun, with a particular emphasis on solar analogues. These dwarf stars are similar to the Sun in terms of mass ( $1 \pm 0.1 M_{\odot}$ ) and metallicity ( $[Fe/H] = 0 \pm 0.2$ ). However, they are possibly of different ages and belong either to OCs or to the field. It is now well established that the photospheric Li abundance of these objects decreases along the main sequence, with indications that slower rotators and/or more metallic solar analogues exhibit lower Li content (Soderblom et al. 1993, King et al. 1997, Takeda et al. 2007, do Nascimento et al. 2013, Monroe et al. 2013, Meléndez et al. 2014, Martos et al. 2023, Lubin et al. 2024). Important Li scatter among field solar analogues at a given age was usually reported, with some suspicion that part of it was due to small differences in mass, metallicity, and evolution status of the sample stars, impacting their Li-depletion history. In particular, based only on spectroscopy and on the isochronal method with very limited applicability to dwarfs (Lebreton et al. 2014, Morel et al. 2021, and references therein), the Sun has long been thought to have the lowest Li abundance among field solar twins of similar age (Carlos et al. 2020, and references therein). This was demonstrated erroneous, thanks to asteroseismology which provides precise and accurate values for the age, mass and radius of oscillating stars (Chaplin et al. 2014, Aerts 2021, Morel et al. 2021, Castro et al. 2021). The combined spectroscopic, photometric, and seismic analysis of solar analogues observed with *Kepler*, which also provided their surface rotation periods (hence alleviating the observational restriction related to the spectroscopic determination of  $vsini$ ), demonstrated that the solar Li and rotation rate appear normal for a star like the Sun at its age (Beck et al. 2017).

**2.2.2. Dwarf stars in open clusters.** Open cluster (OC) stars are supposed to be coeval and to share the same initial composition, with both age and composition varying from one cluster to another. Starting with the seminal work of Herbig (1965) and Wallerstein et al. (1965), their study has depicted the Li depletion history in Pop I dwarf stars, and demonstrated its dependence with spectral type. The well-known and ubiquitous Li- $T_{\text{eff}}$ -age patterns for AFGK dwarf stars are clearly identifiable in Fig. 2 that shows Li data in several OC of different ages and  $[Fe/H]$ . The effective temperature is a proxy for stellar mass at a given metallicity and age, starting from hotter and more massive A- and F-type stars on the left of the plot and moving to cooler and less massive G- and K-type stars towards the right.

The highest Li abundances are found in the youngest systems, as well as in A- and F-type stars with  $T_{\text{eff}} \geq 6800K$  (Boesgaard & Tripicco 1986, Hobbs & Pilachowski 1986, Burkhart & Coupry 1989, 2000, Randich et al. 1997, 2020, Sun et al. 2023). Those lie along a plateau

**Classical stellar model:** Stellar evolution model with convection as the only mechanism for the mixing of chemicals in a star

**A(Li):**  
 $\log_{10}(N_{\text{Li}}/N_{\text{H}}) + 12$   
 where  $N_{\text{Li}}$  and  $N_{\text{H}}$  are the number density of lithium and hydrogen respectively

**Population I:** Pop I stars are typically younger than 10 Gyr, metal rich ( $[Fe/H] > -1$ ), and located near the plane of the Galactic disc

**Population II:** Pop II stars are 11-13.5 Gyr old, metal poor ( $[Fe/H] < -1$ ), and are found in the Galactic halo

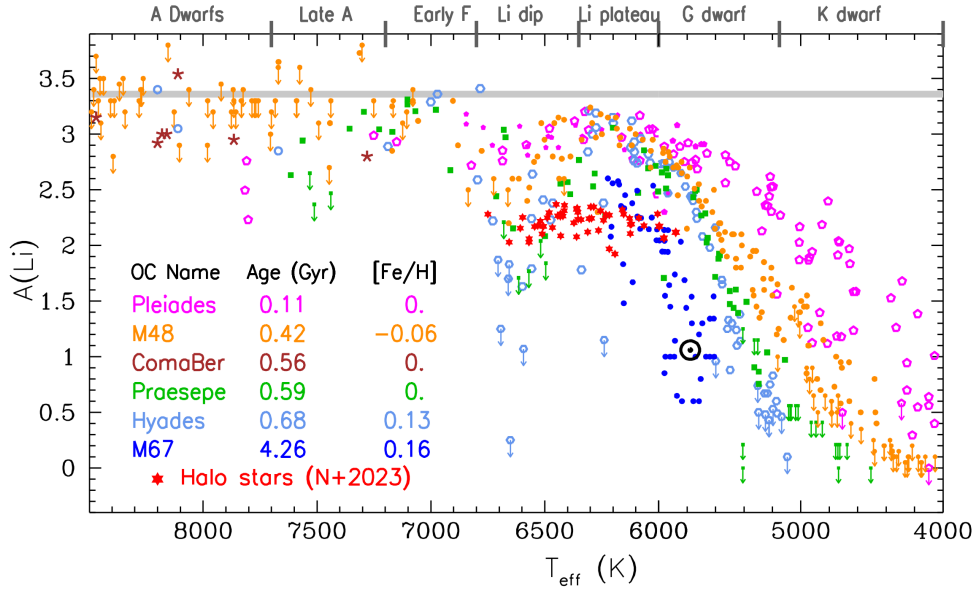


**Figure 2**

Li abundances in OC and halo dwarf stars as a function of effective temperature. The stellar types and the main Li abundance patterns discussed in the text are indicated. The OC data are: for Pleiades from Boesgaard et al. (2003, filled magenta) and Bouvier et al. (2018, open magenta), for M67 from Pace et al. (2012, filled blue), for Praesepe from Cummings et al. (2017, green squares), for Coma Ber from Burkhardt & Coupry (2000, brown asterisks) and for M48 from Sun et al. (2023, orange). The Li abundances of Pop II halo dwarfs are from the Norris et al. (2023) sample, as cleaned in Borisov et al. (2024a). The grey line indicates the meteoritic Li abundance. The temperature scales vary among the studies and have not been homogeneised here.

close to the meteoritic value, independently of the age of the OC. Relatively few abundance determinations are available in this  $T_{\text{eff}}$  range, as the primary abundance diagnostic, the Li I 670.8 nm resonance line, is weaker in hotter stars. Excessive line broadening further complicates spectroscopic analyses in fast rotators ( $v\sin i > 25 \text{ km s}^{-1}$ ), which constitute the majority of A- and F-type stars. This explains why in Fig. 2 most of the A-type stars in M48 from Sun et al. (2025b)'s sample have Li upper limits. Cooler dwarf stars exhibit lower levels of lithium in their photospheres as OC age.

A drop-off in the Li content centred around 6500-6700 K is clearly visible in Fig. 2. The so-called Li dip appears in OC older than  $\sim 150$ -200 Myrs (Wallerstein et al. 1965, Boesgaard & Tripicco 1986, Hobbs & Pilachowski 1988, Balachandran 1995, Burkhardt & Coupry 2000, Pasquini et al. 2001, Steinhauer & Deliyannis 2004) but not in younger ones (Sun et al. 2023, and references therein). No significant alteration of the Li distribution within the dip is detectable in clusters older than the Hyades ( $\sim 700$  Myrs; Anthony-Twarog et al. 2009). This pattern thus builds up early on the main sequence. Importantly, the dip's position occurs at nearly identical  $T_{\text{eff}}$  across a wide range of metallicity, and corresponds to higher mass stars in higher metallicity OC (Cummings et al. 2012, François et al. 2013). In older OC like M67 or NGC 3680, Li dip stars have left the main sequence, but the analysis of slightly evolved subgiants originating from the  $T_{\text{eff}}$  location of the dip

confirms that this pattern is universal (Balachandran 1995, Pasquini et al. 2001, Deliyannis et al. 2019).

On the cool side of the dip, Li rises with a tight Li- $T_{\text{eff}}$  relation (with only a few binaries falling below, Cummings et al. 2017) up to another plateau (between  $\sim 6350$  and  $\sim 6000$  K), hereafter the Pop I Li plateau. Its Li value decreases uniformly with age and is lower than the plateau above the high-temperature boundary of the Li-dip.

Moving towards lower effective temperature, lower mass late-G and K-type stars exhibit Li depletion already in the youngest OC before their arrival on the zero age main sequence (ZAMS; i.e., those stars undergo moderate Li depletion on the pre-MS, see the data for NGC 2547 and the Pleiades in Fig. 2), as well as later on the main sequence. The Li depletion levels are strongly  $T_{\text{eff}}$ -dependent at all ages, with steeper Li- $T_{\text{eff}}$ -depletion trend in more metal-rich clusters at a given age (Zappala 1972, Cayrel et al. 1984, Sestito & Randich 2005, Cummings et al. 2012). Finally, and in contrast to the findings observed on the cool side of the Li-dip, G-dwarf binaries align perfectly with the trends observed for single stars (not shown in Fig. 2, but see Sun et al. 2023).

**2.2.3. Population I field dwarf stars.** The Li- $T_{\text{eff}}$ -age patterns observed in OC have been clearly identified in Pop I field stars, first from small stellar samples (Balachandran 1990, Lambert et al. 1991) and more recently with large spectroscopic surveys. The Li dip was clearly identified from GALAH data as a significant overdensity of stars with Li upper limits in the specific region of the Kiel diagram spanning the evolution path of Li-dip stars ( $T_{\text{eff}}$  between  $\sim 6300$  and  $6600$  K, surface gravity  $\log g$  between 3.8 and 4.3,  $[\text{Fe}/\text{H}]$  between -1 and +0.5; Gao et al. 2020). It is thus clearly established that the Li dip is a universal main sequence phenomenon and that it is confined to the same effective temperature range for all metallicities at which it is potentially observable (i.e., down to  $[\text{Fe}/\text{H}] \sim -1$ ; more metal-poor stars originating from the hot side of the dip have already left the main sequence). In addition, Gao et al. (2020) retrieved the different Li-depletion regimes for the groups of main sequence stars that are, respectively, cooler and hotter than the Li dip. The warm group exhibits no significant Li depletion as they age along the main sequence, independently of their metallicity, while the Li depletion in the cool group is strongly dependent on age,  $T_{\text{eff}}$ , and metallicity.

**Li dip:** Drop-off in the Li photospheric abundances of F-type main sequence stars centred around 6500-6700 K and observed at all  $[\text{Fe}/\text{H}] \geq -1$

**Pop I Li plateau:** Relatively constant Li abundance for Pop I dwarf stars with  $T_{\text{eff}}$  between  $\sim 6000$  and  $6350$  K.

**Pop II Li plateau:** Relatively constant Li abundance in the Galactic halo and globular cluster subdwarf stars (including extra-galactic accreted ones) with  $6000 \leq T_{\text{eff}}/\text{K} \leq 6350$  and  $[\text{Fe}/\text{H}] \leq -0.7$

**2.2.4. Observational evidence of Li depletion in Population II Galactic and extra-galactic dwarf stars.** The discovery by Spite & Spite (1982) of a relatively constant Li abundance in Pop II halo subdwarf stars with  $[\text{Fe}/\text{H}]$  between -0.7 and -2.5 and  $T_{\text{eff}}$  between  $\sim 5800$  K (or 6000 K, depending on the adopted temperature scale) and 6300 K (6500 K) has opened up a large number of discussions linking BBN (§ 4.2), Galactic chemical evolution (§ 5.1), and stellar physics (§ 3). Several surveys of Li in MS turnoff halo stars have investigated what is known as the Spite Li plateau (Fig. 2 and 4), with follow up stretching down to  $[\text{Fe}/\text{H}] \sim -6$  (Hobbs & Thorburn 1991, Thorburn 1994, Norris et al. 1994, 2023, Molaro et al. 1995, Ryan et al. 1996, 1999, 2001, Spite et al. 1996, Bonifacio & Molaro 1997, Charbonnel & Primas 2005, Frebel et al. 2008, 2019, Sbordone et al. 2010, Hosford et al. 2010, Caffau et al. 2011, Bonifacio et al. 2012, 2015, Matsuno et al. 2017, Aguado et al. 2019) with an overview of the results presented in Bonifacio et al. (2025). Their findings have prompted extensive debate about the actual abundance level of the Pop II plateau, with a general agreement that

it lies roughly a factor of 3 below the theoretical BBN primordial Li abundance (§ 4.2)<sup>1</sup>, its thickness, the dependencies of Li on  $T_{\text{eff}}$  and [Fe/H], the apparent meltdown at [Fe/H] below -3 and the evidence for an anticorellation between Li and [C/Fe] in the most extremely metal-poor stars. Prior to the review of these points, it is imperative to emphasise that the accurate determination of the actual characteristics of the Li plateau is fundamental for several reasons. On one hand, any possible Li trend with metallicity is important for evaluating the Galactic chemical evolution to the observed Li abundances in stars (§ 5.1), and it can also contribute to a scatter in the data at fixed effective temperature. On the other hand, the level of the plateau as well as any dispersion and/or trend with effective temperature at different metallicities provide key diagnostics on the physical processes that can lead to Li depletion in halo stars with respect to the initial, potentially primordial Li they were born with (§ 4.2). We refer to Charbonnel & Primas (2005) and Norris et al. (2023, and references therein) for discussions about the origin of the observational discrepancies found in the literature and their relations to the assumptions made in the different studies for the determination of the stellar parameters and abundances (e.g. adopted temperature scale, reddening, NLTE and 1-3D corrections). The additional fundamental issue we want to emphasize here is that the derivation of both the Li dispersion and the trends with [Fe/H] and  $T_{\text{eff}}$  (treated separately or in a bivariate analysis) is sensitive to the selection of the stellar samples and to the treatment of the Li “outliers” when drawing conclusions. This is where astrometry and additional spectroscopic information become crucial in order to address questions relating to the Li plateau, as illustrated by a couple of examples below.

Using Hipparcos parallaxes to determine the evolution stage of a halo sample from the literature, Charbonnel & Primas (2005) showed that most stars with Li under-abundances below the plateau in the [Fe/H] range between -1 and -3.5 were actually slightly evolved, post turnoff stars originating from the hot side of the plateau, whose inclusion resulted in an artificial increase in the Li dispersion previously derived for turnoff stars. More recently, using Gaia DR3 to characterise halo dwarf stars from GALAH DR3 (Buder et al. 2021) combined with the literature sample homogeneously analysed by Norris et al. (2023), Borisov et al. (2024a) confirmed that the Li plateau extends down to [Fe/H]=-6 for stars with  $T_{\text{eff}}$  above 5800 K, with all the Li deficient stars being peculiar anomalous objects.

In particular, and as underlined by Norris et al. (2023), the most metal-poor ([Fe/H]  $\leq$ -4.5) stars of the currently available samples are both Li-poor ( $A(\text{Li})$  between 0.5 and 2.2) and extremely carbon-rich (CEMP with [C/Fe]> 3.5), with an anticorrelation between Li and C indicating that they were probably already Li-deficient at birth due to close environmental effects. The apparent Li meltdown in the [Fe/H] range between -4.2 and -3 is also accompanied by C enrichment, with [C/Fe] up to +3.2. These stars are thus not relevant to the original Li abundance patterns at the earliest times in the young Milky Way. When CEMP-s and CEMP-no stars are excluded from the analysis, there is no (or only very little) evidence for a bending of the Li plateau at low metallicity. Instead, the constancy of the plateau in the most metal-poor regime is sustained by the finding of the most Fe-poor (< -5.8) Li-plateau star, J0023+0307, which is not a CEMP star (Aguado et al. 2019, Frebel et al. 2019). Although they should be very rare, we are anticipating that the Li abundance in extremely metal-poor dwarfs with  $T_{\text{eff}}$  above  $\sim$ 6000 K and no significant C-enrichment should lie on the Li plateau. Finally, studies of turnoff globular

---

<sup>1</sup>For dwarf stars with  $T_{\text{eff}} > 6000$  K and  $-2 < [\text{Fe}/\text{H}] < -1$ , Norris et al. (2023) derive  $\langle A(\text{Li}) \rangle = 2.322 \pm 0.013$ , with  $\sigma(A(\text{Li})) = 0.078$ .

cluster stars reported Li abundance in these objects consistent with the halo plateau value (Lind et al. 2009, Nordlander et al. 2024). Any successful theoretical explanation of Li depletion must explain both halo and GC multiple stellar populations<sup>2</sup>.

The observation of Li in unevolved stars in galaxies outside the Milky Way is, at present, unfeasible. However, successive mergers with dwarf galaxies have brought some of these originally extragalactic stars into the Galactic halo, giving access to extragalactic Li abundances. The first extra-galactic Li plateau was evidenced in the globular cluster-like stellar system Omega Cen, which is thought to be the stripped core of a dwarf galaxy. The Omega Cen plateau lies at the same Li abundance level than in *in situ* Galactic halo stars, and it spans a wide range of metallicities that overlap with that of the Spite plateau (Monaco et al. 2010). Thanks to the extraordinary performance of Gaia astrometry and associated spectroscopic and deep photometric surveys, the same Li plateau was found in *Gaia*-Sausage-Enceladus, a disrupted dwarf galaxy after collision with the Milky Way about 10 Gyr ago (Molaro et al. 2020, Simpson et al. 2021), and in the S2-Stream (Aguado et al. 2021). The universality of the Li plateau for  $[\text{Fe}/\text{H}]$  lower than  $\sim -1.0$  in other galaxies, regardless of their type and their likely different star formation and chemical enrichment histories, implies that this feature does not result from environmental effects. This excludes scenarios calling for the astration of a large fraction of the interstellar medium (ISM) of galactic haloes by a first generation of massive stars that would have effectively destroyed Li before the formation of Galactic and extragalactic halo dwarf stars observed today (Piau et al. 2006, Miranda 2025). In addition, such a process would lead to an important early overproduction of CNO elements, which is not observed in halo stars (Prantzos 2010) and to a strong depletion of the much more fragile deuterium in the Galaxy, which is not observed either.

---

**Astration:** The modification of the composition of interstellar gas after it is re-ejected by a star

---

### 2.3. Observational evidence of Li dilution and depletion in evolved low-mass stars, and the case of Li-rich red giants

**2.3.1. Li dilution and depletion in evolved low-mass stars.** When low-mass stars leave the main sequence, they evolve towards the subgiant and red giant phases. Their radius increases, they become redder and brighter, and their surface rotation drops, facilitating the Li abundance determination in these objects (McKellar 1940). On the other hand, their convective envelope deepens towards internal layers where Li was fully destroyed by proton captures in the earlier phases of their evolution. Consequently, the surface Li abundance decreases due to dilution with Li-free material during the so-called first dredge-up (1DUP; Iben 1967; Sect.3.5; McKellar 1940, Alschuler 1975, Lambert et al. 1980, Lèbre et al. 1999, Mallik et al. 2003, Canto Martins et al. 2011). During that phase, the convective envelope also dredges-up deep layers where the CN-branch occurred during the main sequence, leading to a decrease of the surface C/N and carbon isotopic ratios (Charbonnel 1994). These LiCN evolutionary dilution patterns were clearly identified among FGK field red giants over a wide metallicity range (Shetrone et al. 1993, Aguilera-Gómez et al. 2023), as well as in open clusters (Pilachowski 1986, Sneden & Pilachowski 1986, Pilachowski et al. 1988, Gilroy 1989, Pasquini et al. 2004, Böcek Topcu et al. 2015, Smiljanic et al. 2016, Anthony-Twarog et al. 2018, Deliyannis et al. 2019) and in globular clusters (Lind et al. 2009, Aoki et al. 2021).

---

<sup>2</sup>Due to lack of space we do not tackle the question of Li in the multiple stellar populations of globular clusters and we refer to Gieles et al. (2025) for references and discussion.

After the end of the 1DUP, the surface Li abundance stays constant as the low-mass stars climb the low luminosity part of the RGB, until they reach the location of the so-called RGB bump. There, a second drop of the Li surface abundance occurs, simultaneous to a second drop of the carbon isotopic ratio, when the corresponding data are available (Charbonnel et al. 1998, Gratton et al. 2000, Lind et al. 2009, for both Pop I and Pop II (including GC) giants). Both the Li depletion and the decrease of the carbon isotopic ratios are observed to be more drastic when the mass and/or the metallicity of the RGB stars are lower. This trend is corroborated by asteroseismology coupled to spectroscopy (Coelho et al. 2024, Lagarde et al. 2024). More insight on the evolution of Li in evolved stars of different initial masses comes from large spectroscopic surveys combined with Gaia data, which confirm the global trends described above (Charbonnel et al. 2020, Magrini et al. 2021, Wang et al. 2024). This includes the discovery of Li-rich giants discussed below, the nature of which is strongly debated.

**2.3.2. Li-rich red giants.** In principle, the criteria for classifying a giant star as Li-rich is very simple. It is a star that is evolved enough to have completed the 1DUP, and which exhibits a photospheric Li abundance significantly higher than that of its evolved counterparts as well as theoretical predictions at the same evolution stage. Historically, Li-rich TP-AGB stars have been treated separately (Sect.4.3), and the stars we discuss here are potentially on the RGB, in the red clump or the horizontal branch, or on the early-AGB. Following the unexpected discovery of some of these objects (Wallerstein & Sneden 1982), systematic surveys were carried out to search for them among field giants (Brown et al. 1989, Mallik 1999, Jasniewicz et al. 1999, Kumar et al. 2011, Martell & Shetrone 2013), with a recent acceleration in the domain thanks to Gaia-ESO, GALAH and LAMOST (Casey et al. 2016, Gao et al. 2019, Cai et al. 2023, Ding et al. 2024). In some cases, the selection function or the observing strategy have precluded the precise determination of the frequency of Li-rich red giants and its possible dependence with parameters like the stellar mass or metallicity. However, what is usually found in the literature is that  $\sim 1-2\%$  of field G and K giants have enhanced photospheric lithium abundances with respect to their Li-depleted counterparts. Of those,  $\sim 3\%$  have Li above the meteoritic value, with only a handful exhibiting  $A(\text{Li}) > 4$ .

These estimates and their interpretation about the nature of the (super-) Li-rich giants should be taken with great caution. The popular Li threshold value of 1.5 corresponds roughly to the canonical post-1DUP value predicted by classical models of solar metallicity stars with masses  $\sim 1.25 - 1.5 M_{\odot}$  (Iben 1967), assuming they all formed and left the main sequence with the Li meteoritic value. This simplification has resulted in a significant amount of confusion in the identification of giants that are really abnormally rich in Li, for the following reasons. First and as explained in Sect. 2.2, stars don't leave the main sequence with their original Li photospheric abundance, and Li depletion on the main sequence is both mass and metallicity dependent; therefore, post-1DUP Li abundances are expected to vary accordingly. Second, isochronal determination of the mass of red giants applied in most studies is highly uncertain and the asteroseismic mass-determination is still limited to small number of stars (Serenelli et al. 2021, Warfield et al. 2024, Casali et al. 2025). Nevertheless, asteroseismology facilitates the differentiation of red clump stars undergoing central He-burning from RGB and early-AGB stars that are undergoing H- (and eventually He-) shell burning (Bedding et al. 2011, Vrard et al. 2025). Last but not least, the distribution of the masses of today's giants in any field star sample is different in the different regions of the HRD, and it also depends on the metallicity and the age

of the populations investigated. Consequently, the interpretation of Li data from large surveys requires the understanding of the mass distribution and a careful consideration of the selection effects. This is elegantly illustrated by Chanamé et al. (2022) who revisited the Li data from GALAH DR2 for evolved stars. Assuming that all red clump (RC) stars from the same sample have masses around  $1 M_{\odot}$ , Kumar et al. (2020) had previously claimed that all these stars have high levels of Li for their evolution stage (i.e., are Li-rich), calling for a Li production phase between the RGB tip and the clump. Chanamé et al. (2022) demonstrated, however, that the Li abundances observed in RC stars are normal when one considers a realistic stellar mass distribution in the sample together with a proper mass-dependent Li depletion on the main sequence and the corresponding post-main sequence dilution. More precisely, they predicted a large fraction of very low Li abundances (hence a large number of upper limits) from low-mass RC progenitors, and higher Li abundances from higher mass ones. These trends have been confirmed with GALAH DR4 (Buder et al. 2025). Therefore, their conclusion that “*there is no evidence among clump giants of an unknown Li production mechanism occurring between the upper RGB and the horizontal branch for low-mass stars*”, at odds with Kumar et al. (2020)’s conclusion, is robust.

Given the issues and the example discussed above, important efforts must be devoted to ascertain the mass and the position in the HRD diagram of Li-rich and super Li-rich giant candidates, potentially with asteroseismic clues on their evolution phase, and with the determination of their carbon isotopic ratio, which is an additional indicator of these factors (Lagarde et al. 2024, and references therein). The improvement in the determination of the parallaxes and luminosities thanks to Hipparcos and Gaia astrometry provided some evidence that Li-rich and super Li-rich cool and low-mass giants (typically below  $\sim 2 M_{\odot}$ ) are primarily located in specific regions of the colour-magnitude diagram, namely close to the RGB bump or on the early-AGB (Charbonnel & Balachandran 2000, Kumar et al. 2011, Kowkabany et al. 2024). When available, the low values of  $^{12}\text{C}/^{13}\text{C}$  found in these objects corroborate this finding (Balachandran et al. 2000, Zhou et al. 2018), suggesting internal Li production to replenish Li at the surface of red giants during very brief evolution phases. In a few OC, Li-rich giants with similar CMD location have been found (Anthony-Twarog et al. 2013). Conversely, some studies have identified Li-rich giants in various locations along the RGB, which lends support to the hypothesis of an external contribution of Li, possibly resulting from the engulfment of sub-stellar objects (Casey et al. 2016, Delgado Mena et al. 2016, Aguilera-Gómez et al. 2016). This phenomenology should be scrutinized further through a fully consistent analysis of the available data accounting for all the possible observational and sampling biases, including cluster membership.

We conclude with 2MASS J05241392-0336543, which is the most Li-enhanced giant star discovered to date (A(Li), 3D, NLTE =  $6.15 \pm 0.25$ ; [Li/Fe]= $+7.64 \pm 0.25$ ; Kowkabany et al. 2024). It is very metal-poor ([Fe/H] =  $-2.43 \pm 0.16$ ), C-enhanced ([C/Fe]=  $+0.51$ ), and it has a low  $^{12}\text{C}/^{13}\text{C}$  ( $10 \pm 3$ ). Given its relatively low  $T_{\text{eff}}$ , it is definitively not undergoing central He-burning on the horizontal branch (the equivalent of the clump for metal-poor giants). Instead, it is either a RGB star located just above the bump, or on the early asymptotic giant branch (e-AGB). This provides evidence for fresh  $^7\text{Li}$  production and excludes both preservation of primordial Li and planetary accretion as viable scenarios for the formation of this red giant star with the highest ultralithium enhancement.

### 3. HOW DO STARS DEPLETE LITHIUM

*“The history of our attempts to understand the abundance of lithium in the Sun has had its share of vicissitudes”* (Weymann & Sears 1965). After the acknowledgement, in 1965, that the Li depletion history in the Sun and in low-mass dwarf stars could not be explained by the so-called classical theory of stellar evolution (in brief, the surface convection zone is much shallower than the Li preservation layers; Sect. 2.1 and Fig. 2), several physical processes have been considered for reproducing the observations. The theoretical challenge was (and still is) threefold: 1) to identify the physical processes that transport chemicals and angular momentum in stellar interiors, and their possible interactions; 2) to describe them in a way that could be portable into 1D stellar evolution codes; and 3) to test them consistently across the HRD, both in terms of spectral type and evolution phases, and over the metallicity ranges where data are available. We focus on those mechanisms whose consideration to solve self-consistently the stellar Li puzzles appears to still hold relevance today.

#### 3.1. Atomic diffusion and competing processes

Atomic diffusion of different species against the hydrogen background is mainly led by the gradients of pressure or gravity, of concentration, and of temperature, and by radiative acceleration, which can be computed from first principles (Michaud et al. 2015, and references therein). It is considered as a “standard” process in the modelling of low-mass stars, as it lowers their lifetime (VandenBerg et al. 2002). It is however widely recognized that, in the vast majority of stars, including the Sun as supported by helioseismology (Christensen-Dalsgaard 2021, and references therein), the effects of atomic diffusion are smoothed out, at least partly, by competing macroscopic processes. Li has played (and is still playing) a key role in their identification.

If the radiative layers underneath the convective envelope of dwarf stars were totally stable, the efficiency of atomic diffusion increases (i.e., its timescale decreases) with decreasing density, hence with increasing stellar radius. Hence, while the timescale for atomic diffusion in the Sun is too long to explain the solar Li, it should significantly alter the photospheric composition of hotter stars. In particular, the external H-He convection envelope gets rapidly shallower as  $T_{\text{eff}}$  increases between  $\sim 6000$  and  $7000$  K. This led to Michaud (1986)’s original suggestion that the Li dip centered around 6700 K could be shaped by atomic diffusion, with gravitational settling causing the drop in Li on the cool side of the dip as the stellar convection envelope shrinks, and radiative levitation or mass loss leading to the rise on the hot side of the dip. Three serious drawbacks were however quickly identified. First, the expected concomitant abundance variations of heavier elements (C, N, O, Mg, Si, Cr, Mn) are not observed across the  $T_{\text{eff}}$  range of the Li dip (Garcia Lopez et al. 1993, Varenne & Monier 1999, Takeda et al. 2013). Second, the diffusion timescales would lead Li to settle and accumulate in a buffer zone below the convection envelope; Li should thus be dredged-up when the stars enter the Hertzsprung gap, which is not observed in field and open cluster subgiants (Pilachowski et al. 1988, do Nascimento et al. 2000, Sun et al. 2025a). Third, in the case of pure atomic diffusion, Li, Be, and B would sink below the convective envelope at very similar rates. While a Be-dip was evidenced in several OC at the same  $T_{\text{eff}}$  as the Li dip, it is much shallower, and B is hardly depleted in Li and Be dip stars (Fig.3.1; Boesgaard et al. 2022, and references therein). Explanations relying on a transport process leading to the nuclear destruction of Li and Be in F-type stars are

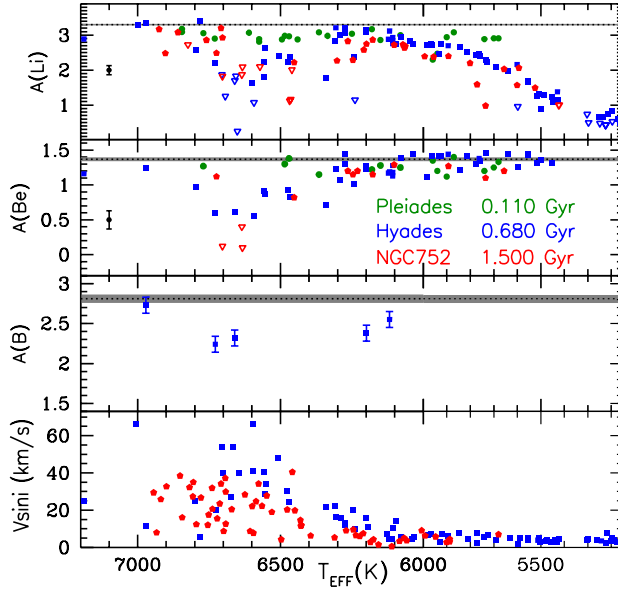


**Figure 3**

Abundances of Li (*top*), Be (*second from top*), B (*third from top*) and  $v\sin i$  (*bottom*) versus  $T_{\text{eff}}$  for dwarf stars in the Pleiades (green dots), Hyades (blue squares) and NGC752 (red pentagons), with upper limits indicated by open downturned triangles. Horizontal grey lines indicate proto-solar values. Figure adapted from Boesgaard (2023) and references therein.

thus favoured, with strong constraints on its efficiency and radial extension coming from the Li/Be/B ratio inside the dip. A substantial body of evidence has emerged indicating that rotation-induced processes are likely the culprit.

Another sign that some mild transport process counteracts atomic diffusion in low-mass dwarf stars of similar effective temperature, whatever their metallicity, is the flatness of the Pop II Li plateau (Sect. 2.2.4). With atomic diffusion alone, the Li depletion would increase with effective temperature (Vauclair 1988, Deliyannis et al. 1990, Proffitt & Michaud 1991). The introduction in stellar evolution models of a very simple turbulent transport coefficient in the radiative interior is all that is required to produce a flat Li abundance plateau as observed in Pop II dwarfs (Richard et al. 2002, 2005). When the parameters describing mild turbulence are adjusted to reproduce the small abundance variations of metals (Mg, Ca, Ti, Fe) between turnoff and subgiant stars in globular clusters, Li depletion by  $\sim 0.2$  to  $0.5$  from its original abundance is predicted (Korn et al. 2006, Gruyters et al. 2016, Nordlander et al. 2024, Borisov et al. 2024a). There are numerous indications that rotation is at the origin of the mixing process involved.

---

**Type I rotating models:**

Models of rotating stars where the transport of angular momentum and of chemicals is driven by meridional circulation and shear turbulence.

**Type II rotating models:**

Models with additionally considered magnetic fields and/or internal gravity waves for the transport of angular momentum and chemicals

---

### 3.2. Type I rotating models

Rotation was suggested to play a dominant role in shaping the Li behaviour in low-mass stars since Boesgaard (1987) noticed that the  $T_{\text{eff}}$  of the Li dip in the Hyades is associated with the drop in rotation velocities that was first evidenced by Kraft (1967), as illustrated in Fig. 3.1. This sharp decline in rotational velocities of main-sequence stars later than spectral type F4V is related to the transition between hotter stars with envelopes in radiative equilibrium and cooler stars with well-developed subsurface H-He convection zones. In the latter ones, magnetically coupled winds are responsible for the deceleration observed early on the sequence (Wilson 1966, and more details below). The coincidence between the Li and Be dips and the rotation drop (i.e., the efficient extraction of angular momentum by the stellar winds) was confirmed in several OC (Boesgaard et al. 2016, Cummings et al. 2017).

Li has played a key role to test the so-called Type I rotating models that are based on Zahn (1992)'s pioneering developments (Palacios 2022, and references therein). In this framework, the modelling of rotation-induced mixing is inextricably linked to the modelling of the angular momentum transport within the star, which is dominated by the Eddington-Sweet (large scale) meridional circulation and by shear instabilities. The circulation is driven by the loss (or the gain) of angular momentum through magnetic winds (or through accretion). The resultant internal rotation is non uniform; a baroclinic state ensues, with the temperature varying with latitude along isobars. Additionally, the differential rotation is expected to trigger hydrodynamical turbulence through various instabilities (shear, baroclinic, and multidiffusive instabilities). As the turbulence acts to reduce its cause (i.e., the angular velocity gradients), it can be modelled as a diffusive process which transports both angular momentum and chemicals together with meridional circulation (Chaboyer & Zahn 1992). In Zahn's framework, the main sources of turbulence are vertical and horizontal shears. Several prescriptions have been proposed for the corresponding diffusion coefficients, some based on multi-D numerical simulations (Palacios 2022, and references therein).

Those must be coupled self-consistently to the treatment of meridional circulation as an advective process in stellar evolution models (the advection term for meridional circulation is very important, as it allows angular momentum to be transported up the gradient of angular velocity  $\Omega$ ). The resulting chemical mixing properties are directly related to the angular velocity gradients, which also depend on how angular momentum is extracted from the stellar surface, depending on its  $T_{\text{eff}}$ .

A and F-type dwarf stars with  $T_{\text{eff}}$  above  $\sim 6800$  K are not efficiently spun down by a magnetic torque (see  $v\sin i$  in Fig. 3.1), as their convective envelope is either nonexistent or too shallow for magnetic generation via a dynamo process. A small flux of angular momentum resulting from the respective contraction and expansion of their core and surface is however present in their interior, with a stationary regime where shear turbulence and meridional circulation counterbalance each other, and with mean molecular weight gradients below the convective envelope also playing a stabilizing role. Depending on the stellar rotation rate, the resulting weak mixing can counteract the effects of atomic diffusion on metals (Talon et al. 2006, Deal et al. 2020), while preserving the photospheric Li along the main sequence. This is supported by the fact that Am stars, which are relatively slower rotators than normal A stars, are Li-deficient compare to A stars (by a factor of  $\sim 3$ ), and show uniform over- and underabundances of metals (Burkhart & Coupry 2000).

The convective envelope of dwarf stars becomes deeper through the  $T_{\text{eff}}$  range between

$\sim 6900$  and  $6500$  K. The surface dynamo can sustain a magnetic torque which spins down the outer stellar layers (Fig.3.1). The resulting angular momentum extraction induces an increase of the angular rotation gradients between the stellar core and surface, resulting in stronger meridional circulation and shear turbulence and associated mixing. As a consequence, stars with cooler  $T_{\text{eff}}$  are expected to experience larger destruction of both Li and Be, as observed in the dip. Early Type I rotating models that use specific prescriptions for vertical and horizontal shears (Talon & Zahn 1997, Zahn 1992, respectively) are able to very well reproduce the blue side of the Li and Be dips as it deepens in open clusters of increasing age (Talon & Charbonnel 1998, Charbonnel & Talon 1999, Smiljanic et al. 2010).

Finally, the convective envelope is deeper for G-type dwarf stars on the red side of the Li and Be dips ( $T_{\text{eff}}$  lower than  $\sim 6500$  K), resulting in stronger magnetic torques that spin down the outer layers even more efficiently compared to their hotter counterparts (Fig. 3.1). Consequently, the above-mentioned Type I rotating models that fit well the blue side of the dip predict too much Li and Be depletion on the cool side of the dip and in G-dwarfs. Conversely, using different prescriptions for the vertical and horizontal shears (i.e. Zahn 1992, Mathis et al. 2018, respectively) allows for reproducing the cool side of the dip, but not the hot side (Dumont et al. 2021a). This emphasises that one of the major limitations of the treatment of rotation in stellar models comes from the uncertainties on the source and magnitude of shear turbulence. A similar difficulty was emphasised by other studies using different prescriptions for rotation-induced mixing (Castro et al. 2016), or interactions between helium settling and rotation-induced mixing (Théado & Vauclair 2003); in the later case, one of the two free parameters describing the mixing has to be modified by more than one order of magnitude to fit both the hot and the cool side of the dip.

These results support the conclusion by Talon & Charbonnel (1998) that the Li dip corresponds to a transition region where another mechanism participates to the transport of angular momentum together with meridional circulation and shear turbulence, resulting in a different efficiency of the associated mixing of chemicals in dwarf stars of different  $T_{\text{eff}}$  (Sect. 3.4). This conclusion is also directly linked to the main caveat of all Type I rotating models, which predict that the core of solar-type stars would rotate much faster than their surface (Chaboyer et al. 1995, Talon 1997, Eggenberger et al. 2005, Turck-Chièze et al. 2010, Marques et al. 2013). This is ruled out by helioseismology, which revealed that the radiative interior of the Sun rotates almost as a solid-body down to about 0.2 solar radii (García et al. 2007, and references therein). Such asteroseismic precision is not reachable for main sequence stars other than the Sun. However, the degree of differential rotation between the deep layers and the surface could be evaluated for a sample of main sequence stars with masses below  $\sim 1.5M_{\odot}$  observed with *Kepler* (Benomar et al. 2015, 2018, Nielsen et al. 2015), with strong indications that rotation at the surface and in the interior are generally close to each other (within a factor of  $\sim 2$ ), at odds with Type I models predictions.

Considerable theoretical effort has been dedicated to identifying the still-missing transport process(es) for angular momentum (Aerts et al. 2019, and references therein). We focus on the studies that are directly related to the possible consequences for Li depletion in low-mass stars, and call those models Type II rotating models.

### 3.3. Type II rotating models with magnetic instabilities

Large-scale fossil magnetic fields were invoked to account for the rotation profile in the solar radiative interior (Mestel & Weiss 1987, Charbonneau & MacGregor 1993, Barnes et al. 1999). As of today, the difficulty is to simultaneously account for the latitudinal differential rotation in the convective envelope and the thickness of the transition region, known as the tachocline (Spiegel & Zahn 1992, Gough & McIntyre 1998, Zahn 2005), with contradictory insights from different numerical simulations (for a review see Strugarek et al. 2023).

The impact of magnetic instabilities on the internal transport of angular momentum is an interesting alternative, with much focus on the Tayler-Spruit instability (hereafter TSI; Tayler 1973, Spruit 1999, 2002). A small-scale magnetic field may be produced in stably stratified layers in stars through this instability, given that the initial magnetic field of the star is small enough and that the differential rotation, which is invoked as the energy source of the process, reaches a minimum degree (for the latest analytical instability criteria, which is a key issue for a self-consistent modelling of AM transport with the TS dynamo, see Skoutnev & Beloborodov 2025, and references therein). Numerical simulations, which are not yet performed under realistic stellar conditions, provide contrasted results (Braithwaite & Spruit 2017, Petitdemange et al. 2024). The saturation of the instability and the resulting angular momentum transport thus remain poorly understood.

In stellar evolution models, the vertical transport of angular momentum by the TSI in the radiative layers is simulated through the introduction of a magnetic viscosity (i.e., a parametrized diffusion coefficient) in the equation for the transport of angular momentum; it comes in addition to the terms describing the transport of angular momentum by meridional circulation and shear turbulence considered in Type I rotation models. The main issue is that different ad hoc parametric prescriptions are required to reproduce the angular velocity gradients at different phases of the evolution of low-mass stars, i.e., the main sequence, the subgiant phase, and the red giant phases during hydrogen shell burning and core helium burning (Mosser et al. 2012, 2024, Deheuvels et al. 2014, Cantiello et al. 2014, Di Mauro et al. 2016, Triana et al. 2017, Gehan et al. 2018, Fuller et al. 2019, Eggenberger et al. 2022, Moyano et al. 2022, Buldgen et al. 2024), with no clear justification as to why the instability would change from one regime to another. Additionally, the measurement of the rotation of the deep solar core below  $0.2 R_\odot$  using gravity modes is still required to legitimate the credibility of the TSI.

The TSI itself is not expected to transport the chemicals efficiently (Maeder & Meynet 2004). Indeed, while the transport of AM is ensured by the magnetic stresses, the transport of chemicals results from the motions of the fluid, more explicitly by the shear and meridional circulation as in Type I rotating models. However, those mechanisms are themselves regulated by the magnetic instability to the critical value of shear above which it is triggered. As a consequence, a more efficient TSI leads to lower angular velocity gradients, hence to lower mixing efficiency. However, the different formulations for the TSI lead either to the correct depletion of lithium, but resulting in excessive depletion of Be in the Sun, or to no depletion of Li and Be at all (Buldgen et al. 2025). Quoting these authors, this “*casts doubt on the ability to link the observed light-element depletion to the combined effects of shear, circulation, and magnetic Tayler instability*”. To the best of our knowledge, no attempt has been made to reproduce the Li-Teff-age patterns with this mechanism, which anyway does not pass the solar Li and Be test.

Magneto-rotational instabilities, and in particular the azimuthal magnetorotational in-

stability (AMRI), which is a destabilization of hydrodynamically stable differential rotation by current-free toroidal magnetic fields, is an alternative that might be favoured. It extracts its energy from differential rotation, which makes it more efficient for steeper rotation gradients, and ineffective in the case of solid-body rotation. The corresponding turbulent viscosity is expected to be very effective at transporting angular momentum (but much less at transporting chemicals) in a time-dependent way that can explain the observed post-main sequence rotational evolution of low-mass stars (Rüdiger et al. 2015, Spada et al. 2016a, Jouve et al. 2020, Meduri et al. 2024). However, using the expression for the parametric viscosity proposed by Spada et al. (2016a) that depends on the radial rotational shear and which is expected to be consistent with the AM transport by the AMRI, Dumont (2023) showed that Li and Be of main sequence stars can't be reproduced simultaneously. This calls into question the actual relationship between the AMRI instability and the Li and Be depletion history in solar-type stars.

Whether a magnetic instability could account for the Li abundance in dwarf stars of different masses and metallicities remains to be investigated, but the current prescriptions do not pass the Li and Be test in the Sun. The Li dip could once again be the ultimate test, with the pending issues of the triggering of the different magnetic instabilities and the related prescriptions to be included in stellar evolution models, both awaiting for multi-D numerical simulations performed under realistic stellar conditions.

### 3.4. Type II rotating models with magneto-inertial gravity waves

*“The results of this paper, if correct, may be an unwelcome addition to the theory of stellar interiors” (Press 1981, “Radiative and other effects from internal waves in solar and stellar interiors”).*

**3.4.1. The first models including rotation and internal gravity waves.** As with atomic diffusion and rotation-induced processes, the study of the Li dip has highlighted the need to investigate the role of internal gravity waves (IGW) in low-mass stars. As explained in Sect.3.2, this feature falls in a range in effective temperature that corresponds to a transition region for the structural properties of dwarf stars (in particular, the development of the H-He convective envelope) that impact both their surface rotation and Li abundance. It was also stated that it is a transition region where a very efficient transport of angular momentum surpasses meridional circulation and turbulence (Talon & Charbonnel 1998). This turned out to be characteristics of IGW. Using a simplified formalism for bulk wave excitation through Reynolds stresses (more details below), it was shown that the growth of the convective envelope in dwarf stars of both Pop I and Pop II with  $T_{\text{eff}}$  below  $\sim 6600$  K coincides to the growth of the generation and efficiency of IGW in their interior (Talon & Charbonnel 2003, 2004). After the introduction of this excitation formalism together with a semi-analytical framework to treat wave damping and the associated transport of angular momentum together with that due to meridional circulation and shear in stellar evolution codes (Talon & Charbonnel 2005), the results were extremely encouraging. Not only did the models succeed in achieving near uniform rotation in the Sun and solar-type stars, but they could reproduce the behaviour of Li in both Pop I and Pop II dwarf stars, including the Li and Be dips and the flatness of the Li plateau (Talon & Charbonnel 2005, 2010, Charbonnel & Talon 2005a,b, Meléndez et al. 2010).

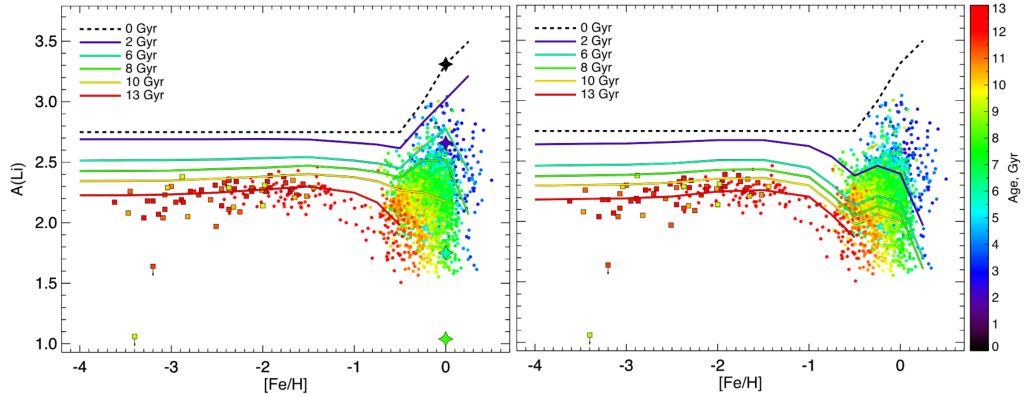


**Figure 4**

Li abundance (3D, NLTE) as a function of  $[\alpha/\text{Fe}]$  for the Norris et al. (2023) and GALAH DR3 sample stars (squares and circles respectively) with colour-coded age. Solid lines show the theoretical Li upper and lower envelopes (left and right panels, respectively) at different ages (in the legend), i.e., the maximum and minimum Li values at a given  $[\text{Fe}/\text{H}]$  and age expected from Type II models with  $5800 \text{ K} < T_{\text{eff}}(\text{ZAMS}) < 6500 \text{ K}$ . The dashed line indicates the initial Li abundance assumed in the models. In the left panel, the four-pointed stars show predictions for  $1 M_{\odot}$  star from models of Dumont et al. (2021b) with age similarly colour-coded. Figure from Borisov et al. (2024a)

**3.4.2. Towards models including rotation, internal gravity waves, magnetism, and their interactions.** If all seemed to be working self-consistently so well when considering rotation-induced processes and internal gravity waves, why weren't these results the end of the quest to understand Li behaviour in low-mass dwarf stars? First, this series of Type II models with IGW were computed with the only combination of prescriptions for vertical and horizontal shears available at that time (Talon & Zahn 1997, Zahn 1992, respectively). This resulted in a perfect shaping of the Li dip while explaining the solar Li. Dumont et al. (2021a,b) showed, however, that this excellent agreement didn't hold anymore when new prescriptions for the vertical and horizontal shears (Zahn 1992 and Mathis et al. 2018 on one hand, and Zahn 1992 and Mathis & Zahn 2004 on the other hand) as validated by direct numerical simulations (Prat & Lignières 2013, Garaud et al. 2017), were included in Type II rotating models. In Dumont et al. (2021a,b), a parametric viscosity (including Spada et al. 2016b's dependence of the angular momentum transport efficiency on the radial rotational shear) was added to meridional circulation and shear to simulate the missing AM transport mechanism; mixing was also parametrised to fit Li in cool dwarfs, including the Sun and solar-type stars.

Interestingly, the same models simultaneously account for the Li plateau (Borisov et al. 2024a) as shown in Fig. 4, offering for the first time a coherent view of Li depletion and angular momentum transport from Pop I to Pop II dwarf stars. However, the new shear prescriptions fail to explain the Li dip even when combined with additional sources for turbulent transport. Consistently with Talon & Charbonnel (2010)'s early findings, the only Type II rotating models of Dumont et al. (2021a) that could reproduce simultaneously the Li dip and the Li behaviour in G-type stars are those including the oldest prescriptions for vertical and horizontal shear turbulence, together with a mass-dependent efficiency for the additional AM transport process, as expected from IGW. Quoting these authors, “*Insight*

*and validation of the different available prescriptions for (...) turbulent shear transport from hydrodynamicists and multi-dimensional numerical simulations (...) are now mandatory in order to overcome this impasse."*

The second reason to revisit Type II models including IGW is that more sophisticated treatment for IGW and their interactions with rotation and magnetic field must be taken into account. IGW naturally occur and propagate in fluids that are stably stratified, with gravity acting as the restoring force. Low-frequency progressive waves have long been considered to play an important role in the redistribution of angular momentum in low-mass stars spun down by a magnetic torque (Press 1981, Schatzman 1993, Zahn et al. 1997, Kumar & Quataert 1997, Talon et al. 2002). They might also trigger chemical mixing (Garcia Lopez & Spruit 1991, Montalban 1994, Montalbán & Schatzman 2000, Young et al. 2003, Rogers & McElwaine 2017). However, this direct wave-induced mixing was usually neglected in Type II rotating models including IGW, where the transport of chemicals is still ensured by the meridional circulation and the shear regulated by the impact of the IGW on the angular velocity gradients (Talon & Charbonnel 2005). Even more importantly, IGW carry angular momentum from the region where they are excited to the region where they are dissipated. A deep understanding of their excitation, propagation, and dissipation mechanisms is thus of key importance.

Third, many studies have focused on the generation of IGW by turbulent convection at the interface between convective and radiative layers in stars (in low-mass stars, the excitation is related to the convective envelope), neglecting the impact of rotation and magnetic fields on wave excitation (here we do not consider tidal excitation but focus on single stars). IGW are excited by two different processes, namely, turbulent pressure in the convective bulk, which is predominant in solar-type stars, and penetrative convection by so-called convective plumes at the interface between the convective and the radiative zones (for a review see Samadi et al. 2015). The existence of those waves is observed in 2 and 3-D numerical simulations (Hurlburt et al. 1986, Andersen 1994, Kiraga et al. 2000, Dintrans et al. 2005, Rogers & Glatzmaier 2005, Alvan et al. 2014, Le Saux et al. 2023), but the extrapolation to the stellar regime remains a challenging task. Consequently, semianalytical prescriptions for excitation have been necessary in a first approach, but they provide only crude descriptions of the generation of IGW in stars. Additionally, the prescriptions that have been used so far in Type II stellar evolution models neglect the action of rotation and magnetism on turbulent convection and therefore on stochastic wave excitation, as studied in numerical and laboratory experiments and theoretical developments (Bessila & Mathis 2024, and references therein). Recently, theoretical progress was achieved to modify the MLT convection formalism to account for rotation and magnetic field (Bessila & Mathis 2025, Rotating and Magnetised Mixing-Length Theory) as well as the formalism for stochastic excitation with both rotation and magnetic field on acoustic modes (Bessila & Mathis, private communication), as required to explain the non detection of acoustic waves in about half of the solar-type stars observed with *Kepler* (Mathur et al. 2019). Extending these formalisms to the case of gravity waves, and testing them in a new generation of Type II stellar evolution models, is a priority.

The next theoretical challenge is to establish realistic prescriptions for the propagation and the dissipation of the waves in the radiative zones, which drive the extraction or deposition of angular momentum in stellar interiors. The first Type II evolution models including angular momentum transport by IGW assumed that radiative damping is the dominant process (Talon & Charbonnel 2005, Fuller et al. 2014). However, the role of critical layers

(when the frequency of the wave is the same as the local rotation frequency; Alvan et al. 2013) and of nonlinear breaking (due to the overturning of the stratification, i.e., convective instability or to the shear of the wave itself, i.e., Kelvin–Helmholtz instability; Barker & Ogilvie 2010, Mathis 2025) have been neglected so far.

Last but not least, low-frequency IGW that transport angular momentum can be modified by the Coriolis acceleration and the Lorentz force. This results in the IGW becoming gravito-inertial (Pantillon et al. 2007, Mathis 2009, Mirouh et al. 2016, Prat et al. 2018) or magneto-gravito-inertial (Dintrans et al. 1999, Rogers & MacGregor 2010, Mathis & de Brye 2011, 2012, Lecoanet et al. 2017).

It is imperative that efforts are pursued to describe the related physics and to develop reliable prescriptions to be included into stellar evolution models. We have no doubt that both the internal rotation revealed by asteroseismology in various eras of the HRD (using the legacy of *Kepler*/K2, Tess, and the future PLATO) and the Li abundance patterns (using the legacy of large spectroscopic surveys) will provide the best constraints to this endeavour. We are confident that the self-consistent treatment of rotation, internal gravity waves, and magnetic field, whose respective impacts have been estimated through simplified prescriptions in already complex stellar evolution models, will confirm that these inter-dependent mechanisms are responsible for the Li-Teff-age-metallicity abundance patterns in low-mass dwarfs.

### 3.5. Lithium depletion along the red giant branch

*Giants with “(...)* Li abundances in agreement with the predictions of standard models are the exception” (Smiljanic et al. 2016). Not surprisingly, the classical and standard stellar evolution models which fail to reproduce the main sequence Li data also fail to explain the Li abundances observed in post-MS low-mass stars (Sect. 2.3.1). In the case of stars originating from the left part of the MS Li dip and belonging both to the field and to OC, Li drops immediately after the turnoff and before the theoretical occurrence of the 1DUP (Mallik et al. 2003, Pasquini et al. 2004, Liu et al. 2014, Deliyannis et al. 2019, Charbonnel et al. 2020). This is related to the fact that the weak mixing that counterbalances atomic diffusion while those stars are on the main sequence enlarges their Li-free region compare to classical models (Palacios et al. 2003, Pasquini et al. 2004, Charbonnel & Lagarde 2010). Additionally, many post-1DUP giants have Li upper limits, which can be explained only if they have undergone Li depletion on the main sequence, in agreement with the main sequence Li data, with rotation-induced mixing being favoured (Sun et al. 2025a). We emphasize that main sequence Li depletion followed by the 1DUP are sufficient to explain the Li depletion observed in stars crossing the Hertzsprung gap and climbing the lower part of the RGB (Charbonnel et al. 2020, Magrini et al. 2021, and references therein), as well as that of Be (Smiljanic et al. 2010). No extra-mixing leading to additional Li destruction is required during these phases. This brings important constraints to the angular momentum transport processes in post-MS stars. Recent asteroseismic observations based on space photometry have uncovered the internal rotation of low-mass subgiants, red giants during hydrogen shell burning, and clump stars during helium burning unambiguously showing that their cores rotate order of magnitudes slower than predicted by Type I rotation models (Deheuvels et al. 2020, Gehan et al. 2018, Mosser et al. 2024, and references therein). Based on semi-parametric models, it has been shown that during the subgiant phase, the angular momentum transport efficiency increases with the mass of the star and decreases as the

star evolves to the bottom of the RGB, and that its efficiency increases with the mass of the star as well as along the climbing of the RGB (Spada et al. 2016a, Moyano et al. 2022, Dumont 2023). Whatever the origin of the angular momentum transport is, it should not affect the photospheric Li abundance in these stars.

Later on along the RGB, however, the additional and sudden photospheric Li drop observed together with a decrease of  $^{12}\text{C}/^{13}\text{C}$  and C/N at the so-called luminosity bump requires the occurrence of a very efficient hydrodynamical instability to transport Li from the base of the convective envelope to its burning region in the outer wing of the hydrogen burning shell where the CN-chain is operating. As of today, the only plausible mechanism to self-consistently explain these observations is the so-called thermohaline instability which is expected to set in at the luminosity of the RGB bump for red giant stars of low-mass that ignite He-burning in their degenerate core through so-called He flashes<sup>3</sup> (Charbonnel & Zahn 2007, Lagarde et al. 2019, Aguilera-Gómez et al. 2023), as corroborated by the seismic analysis of bright red giants observed by CoRoT (Lagarde et al. 2015) and *Kepler* (Coelho et al. 2024). Despite its successes to also explain the Galactic evolution of  $^3\text{He}$  (Lagarde et al. 2012, Balser et al. 2022), the details of the thermohaline mixing are debated (Wachlin et al. 2011, Denissenkov et al. 2009, Denissenkov & Merryfield 2011, Tayar & Joyce 2022), and some observations for red giants belonging to globular clusters are found to deviate from theoretical prescriptions (Angelou et al. 2015, Henkel et al. 2017, McCormick et al. 2023). Several attempts to simulate numerically thermohaline convection have led to contradictory results (Denissenkov 2010, Traxler et al. 2011, Brown et al. 2013). Interestingly, it was found that rotation and/or weak magnetic fields can strongly enhance the vertical transport by this instability, at the level that is necessary to explain the Li behaviour and the concurrent carbon isotopic and C/N ratios changes observed in RGB stars around the luminosity bump (Sengupta & Garaud 2018, Harrington & Garaud 2019, Fraser et al. 2024).

#### 4. PRODUCTION OF LITHIUM IN ASTROPHYSICAL ENVIRONMENTS

In stellar interiors, the minor lithium isotope  $^6\text{Li}$  can be produced directly by thermonuclear reactions between stable isotopes through the reaction  $^9\text{Be} + \text{p} \longrightarrow ^6\text{Li} + ^4\text{He}$ , but negligible amounts of it may survive in any environment. The direct production of the major isotope  $^7\text{Li}$  involves the unstable isotope  $^3\text{H}$  (tritium, lifetime of 12.5 yr) through  $^4\text{He} + ^3\text{H} \longrightarrow ^7\text{Li}$ . Tritium does not exist in stellar interiors but it is formed in the conditions of primordial nucleosynthesis from the capture of the abundant neutrons by deuterium and participates in the formation of  $^7\text{Li}$  in that environment (§ 4.2).

The main mechanism of  $^7\text{Li}$  formation in stars is through the decay of the radioactive isotope  $^7\text{Be}$  which is produced in various stellar environments via  $^3\text{He} + ^4\text{He} \longrightarrow ^7\text{Be}$ . In normal conditions  $^7\text{Be}$  decays through electron capture of a K-shell electron with a lifetime of 53.3 days. Cameron (1955) noticed that in the hot stellar interiors the half-life of  $^7\text{Be}$  is lengthened nearly inversely proportionally to the degree of ionization of its K-shell electrons: at temperatures of  $10^7$ - $10^8$  K its lifetime may be extended to tens of years, allowing  $^7\text{Be}$  to be transported by “circulation currents” from the hot regions to the surface. He argued that this mechanism could conciliate the observations of giant stars showing simultaneously low  $^{12}\text{C}/^{13}\text{C}$  ratios (a signature of CN cycle) and high Li. This mechanism was reinvestigated

---

<sup>3</sup>In more massive stars, this process should not occur on the RGB - since core He-burning starts in non degenerate conditions before the stars could reach the bump - but on the early-AGB.

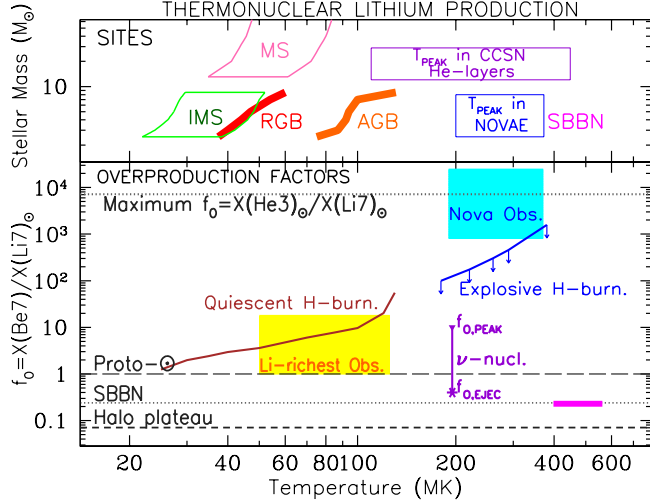


**Figure 5**

*Top:* Stellar astrophysical sites of thermonuclear production of  ${}^7\text{Be}$  with corresponding temperature ranges: core H-burning (horizontally extended from H-ignition on the left to H-exhaustion on the right), in Intermediate Mass Stars (IMS) and Massive Stars (MS), shell H-burning in Red Giant Branch stars (RGB, red) and Hot Bottom Burning in Asymptotic Giant Branch stars (AGB, orange); range of peak temperatures in He-layers of CCSN of 15 to 30  $M_{\odot}$ , where  $\nu$ -induced nucleosynthesis occurs (violet box), novae (blue box) and SBBN (purple).

*Bottom:* Overproduction factors  $f_0$  of  ${}^7\text{Be}$  (with respect to the meteoritic value of  ${}^7\text{Li}$ ). The brown solid curve shows results for quiescent H-burning of solar mixture material at constant temperatures. Li is overproduced, albeit for short timescales: a few  $10^3$  yr for  $T=25$  MK to about a week for  $T=120$  MK. The yellow shaded area indicates observations of Li-richest giant stars. The upper dotted horizontal line indicates the maximum possible value  $f_0$ , with all solar  $\text{He}^3$  turned into  ${}^7\text{Be}$ ; some nova observations indicate higher overproduction (see Fig. 7, right). Blue asterisks indicate maximum  $f_0$  values obtained in nova simulations for indicated peak temperatures (above 180 MK) from Starrfield et al. (2024), while the cyan-coloured shaded area indicates the range from nova observations (Molaro et al. 2023). The vertical violet segment joins peak overproduction  $f_0,\text{PEAK}$  of  ${}^7\text{Li}$  in the He-layers from  $\nu$ -induced nucleosynthesis and corresponding value in the total ejecta  $f_0,\text{EJEC}$  in a  $27 M_{\odot}$  CCSN model (Sieverding et al. 2019). Adopted values (in horizontal lines) are:  $A(\text{Li})=3.39$  for Proto-solar (Lodders et al. 2025, long-dashed line), 2.7 for SBBN (Pitrou et al. 2018, dotted) and 2.2 for halo plateau (Bonifacio et al. 2025, short-dashed).

in Cameron & Fowler (1971) who extended it as to account for the simultaneous presence in S-stars of both Li and s-elements (made in the He-shell of AGB stars). <sup>4</sup>

Fig. 5 presents an overview of the thermonuclear production of  ${}^7\text{Be}$  in various environments. In the top panel, typical temperature ranges in stars of various masses and evolutionary phases are displayed. In the bottom panel, H-burning in stellar cores (main sequence stars), shells (RGBs) and bottoms of convective envelopes (AGBs) is represented by idealized conditions of constant temperature and density, while for the other cases (novae, BBN,  $\nu$ -induced nucleosynthesis) results of recent calculations are shown. The abundance of  ${}^7\text{Be}$  results from the competition between its production and its destruction by proton reactions (electron captures being much slower in such temperatures). In the bottom panel it appears that  ${}^7\text{Be}$  may exist in significant amounts for all the shown temperatures, until exhaustion of the  ${}^3\text{He}$ . The maximum possible mass fraction is the initial mass fraction of

<sup>4</sup>Cameron & Fowler (1971) acknowledge that the Li transport in their scheme follows Cameron (1955). It should be then called - when applied specifically to the case of Li - the "Cameron mechanism" and not the "Cameron-Fowler mechanism" as usually done.

$^3\text{He}$  and this is achieved for temperatures of the order of 200 MK and above (as in nova explosions). This time span is inversely proportional to the density of the site, but the overproduction factor, i.e. its average overabundance w.r.t. proto-solar  $^7\text{Li}$ , is independent of the density. In most cases, the overproduction timespan is much shorter than the evolutionary timescales of stellar interiors and  $^7\text{Be}$  is rapidly destroyed, unless if it manages to escape to cooler regions through the Cameron mechanism. This is the case in both AGB stars and nova explosions, while in the case of BBN and  $\nu$ -induced nucleosynthesis it is rather the rapid cooling of the site that allows the survival of  $^7\text{Be}$ . Before discussing those sites of thermal production of  $^7\text{Be}$ , we turn into a non-thermal mechanism in the next section.

#### 4.1. Spallation reactions in cosmic rays

In view of the fragility of Li, Be and B in stellar interiors, it was suggested that those elements may be produced by high-energy spallation reactions of the more abundant C, N and O nuclei. The acceleration of the spallating nuclei could occur either at the surfaces of flaring solar-type stars (Hayakawa 1955) or of magnetic or T-Tauri star (Fowler et al. 1955, Burbidge et al. 1957), where the low-density environment would preserve their fragile LiBeB products from destruction by thermonuclear reactions. However, Ryter et al. (1970) showed that the release of gravitational energy powering the activity of those stars would be insufficient to produce the observed amounts of those light nuclei in the Galaxy, because a large fraction of that energy would be spent by the energetic nuclei in ionizing the stellar atmospheres.

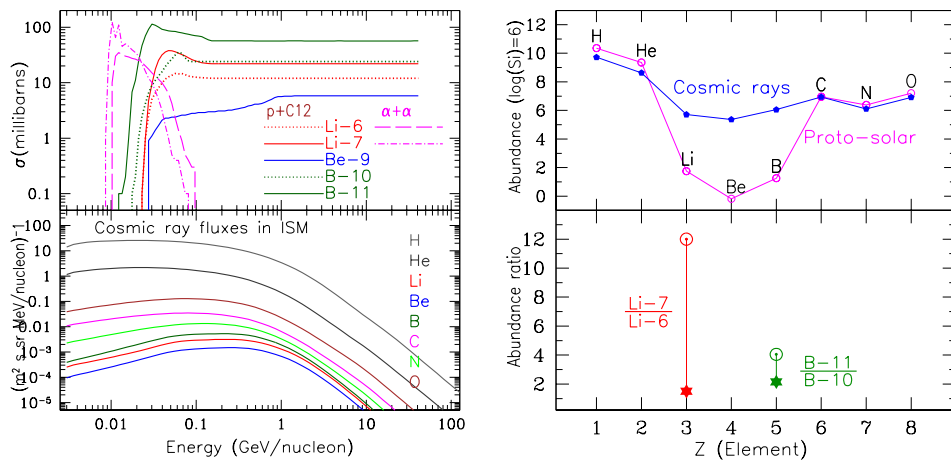


**Figure 6**

*Top left:* Cross-sections of the production of  $^6\text{Li}$ ,  $^7\text{Li}$ ,  $^9\text{Be}$ ,  $^{10}\text{B}$  and  $^{11}\text{B}$  through interactions of  $^{12}\text{C}$  with energetic protons (from Read & Viola 1984) and  $\alpha + \alpha$  reactions (from Mercer et al. 2001). *Bottom left:* Interstellar Galactic Cosmic Ray (GCR) spectra obtained by fitting the Voyager 1 observations with the GALPROP propagation code (Cummings et al. 2016). *Top right:* Composition of the proto-solar system (from Lodders et al. 2025) and in GCR (from Cummings et al. 2016); they are both scaled to  $10^6$  Si atoms. *Bottom right:* Abundance ratios in meteorites (solar symbols) and in GCR (asterisks) observed in PAMELA experiment in ISS (Menn et al. 2018) with  $\text{Li7}$  representing the sum of detected  $^7\text{Li}$  and  $^7\text{Be}$ .

Bradt & Peters (1950) had already noticed that Li, Be and B are present in Galactic Cosmic Rays (GCR) almost at the same level as the abundant C, N and O nuclei, while the LiBeB/CNO ratio is about a million times lower in proto-solar (meteorite) material (Fig. 6 top right). This, along with the measurements of the production cross-sections of LiBeB from CNO (Fig. 6 top left) measured by Bernas et al. (1967), led Reeves et al. (1970) to suggest that Li, Be and B are produced by spallation reactions between the ISM and GCR, during the propagation of the latter in the Galaxy in the  $\sim 10$  Gyr of its life. However, they noticed that the  ${}^7\text{Li}/{}^6\text{Li}$  ratio produced by cosmic rays is  $\sim 8$  times lower than in the meteorites (1.5 vs 12.05 respectively), as shown in Fig. 6 (bottom right): in contrast to the other LiBeB isotopes,  ${}^7\text{Li}$  is largely underproduced in GCR.

Subsequent work, taking into account the injection of accelerated cosmic rays from their sources and their propagation in the Galaxy, in the framework of the so-called "leaky-box" model (Meneguzzi et al. 1971) confirmed the conclusions of Reeves et al. (1970). A similar, albeit less acute problem, was also identified : the  ${}^{11}\text{B}/{}^{10}\text{B}$  ratio in GCR, obtained through the measured cross-sections, is  $\sim 2.2$  compared to its meteoritic value of 4.05 (Fig. 6, bottom right). This difference is much larger than the uncertainties in the production cross-sections or in the meteoritic measurements and, taken at face value, implies that  ${}^{11}\text{B}$  requires another, complementary source in order to fully account for its proto-solar abundance.

The mismatch between proto-solar abundances and the GCR production of the Li and B isotopes requested for alternatives. A low-energy GCR component would favour the production of  ${}^7\text{Li}$  over  ${}^6\text{Li}$  due to the form of the  $\alpha + \alpha$  low-energy cross sections (see Fig. 6) as suggested by Meneguzzi & Reeves (1975), but it would also enhance the ionization of the gas in the acceleration site of GCR, which was not found. Moreover, the Voyager 1 data, obtained at the heliospheric border (Cummings et al. 2016, and Fig. 6, bottom left) indicate that such a component does not exist in the ISM, at least in the local one. The only source suggested so far for  ${}^{11}\text{B}$  is neutrino-induced nucleosynthesis in CCSN, which may also contribute to some extent to  ${}^7\text{Li}$  production (§ 4.5).

Taking into account that  ${}^6\text{Li}$  is exclusively produced by GCR, the contribution of GCR nucleosynthesis to the meteoritic (protosolar) Li abundance (sum of  ${}^6\text{Li}$  and  ${}^7\text{Li}$ ), is  $\sim 20\%$ , i.e. GCR constitute a significant and observationally supported Li source.

## 4.2. Primordial nucleosynthesis

Following the discovery of the CMB in 1965, primordial nucleosynthesis was investigated by Peebles (1966) for the H and He isotopes, then by Wagoner et al. (1967) who considered also heavier nuclei and found substantial production of  ${}^7\text{Li}$ . It is produced by both reactions  ${}^4\text{He} + {}^3\text{H} \rightarrow {}^7\text{Li}$  and  ${}^4\text{He} + {}^3\text{H} \rightarrow {}^7\text{Be}$ . In the former reaction  ${}^3\text{H}$  is obtained through  $\text{D} + \text{n} \rightarrow {}^3\text{H}$ , due to the availability of a large amount of neutrons ( $\text{n}/\text{p} \sim 1/7$ ) at the "freeze-out" of charged-current weak interactions. The reaction with tritium dominates the production of  ${}^7\text{Li}$  at low densities, while at high densities  ${}^7\text{Li}$  production is dominated by  ${}^4\text{He} + {}^3\text{H} \rightarrow {}^7\text{Be}$ . The abundances of  ${}^7\text{Be}$  and  ${}^7\text{Li}$  depend on the competition between the nuclear reaction rates (which depend on the baryonic density) and the expansion rate of the Universe. The rapid cooling of the primordial plasma within a timescale of a few minutes ensures naturally the survival of all isotopes of both  ${}^7\text{Li}$  and  ${}^7\text{Be}$ .

The sensitivity of BBN products (D,  ${}^3\text{He}$ ,  ${}^4\text{He}$  and  ${}^7\text{Li}$ ) to various parameters of the model - in particular, the baryonic density - makes those isotopes important probes of the

physics of the early Universe. The discovery of the "Spite plateau" (see § 2) provided a constraint on the physics of the early universe but it also suggested that SBBN and GCR together cannot make the totality of proto-solar Li, thus making another - most probably stellar - source for that element necessary.

Starting with NASA's WMAP in 2003, BBN results and predictions changed both quantitatively and qualitatively. Instead of roughly evaluating the baryon-to-photon ratio from observations of the light element abundances in old/unevolved systems, this ratio is now obtained to high accuracy from the analysis of the CMB, providing stringent tests of BBN and of physics beyond the Standard Model (Planck Collaboration et al. 2020).

The primordial nucleosynthesis results are currently in excellent agreement with abundance measurements of D in high redshift gas clouds and CMB measurements of baryon/photon ratio (the "triple point" of D, see Cooke 2024, and references therein). However, an important discrepancy persists between the  ${}^7\text{Li}$  value of the halo plateau and the SBBN predictions. The extent and potential causes of that discrepancy were scrutinized over the years: nuclear reaction rate uncertainties (Iliadis & Coc 2020); observational determination of Li abundance in field halo stars or globular clusters (Boesgaard & Deliyannis 2024), particle physics beyond the Standard Model in the early universe (Bertulani et al. 2023, and references therein), or destruction of Li in the atmospheres of halo stars. In § 2.2.4 we argued for the latter solution to the cosmological problem of Li. Recently, Molaro et al. (2024) reported the observation of  $A(\text{Li}) \sim 2.2$ , i.e. the halo plateau, in the Small Magellanic Cloud's gas; if confirmed, this might put in question the stellar solution to the cosmological Li problem.

The cosmologically inferred value of primordial Li,  $A(\text{Li}) = \sim 2.7$ , suggests that primordial nucleosynthesis has a confirmed and significant contribution to the protosolar Li abundance of  $A(\text{Li}) = 3.39$  (Lodders et al. 2025), of the order of  $\sim 20\%$ , which is similar to the one of GCR. This implies that the largest part of protosolar Li,  $\sim 60\%$ , is produced by stars.

### 4.3. Hot Bottom Burning in Asymptotic Giant Branch stars

Despite its fragility,  ${}^7\text{Li}$  can be produced as  ${}^7\text{Be}$  in intermediate-mass stars during the thermal pulse phase on the Asymptotic Giant Branch (TP-AGB) through Hot Bottom Burning in the base of the convective envelope (Scalo et al. 1975). The preservation of  ${}^7\text{Li}$  requires the introduction in the stellar evolution models of a suited time-dependent convective diffusion algorithm for the transport of chemicals in the convective envelope.

${}^7\text{Li}$  can be produced efficiently as long as  ${}^3\text{He}$  is abundant and the HBB proceeds, depending on stellar mass, metallicity and the adopted mass loss rate. Later in the evolution, the surface  ${}^7\text{Li}$  abundance drops again, either because the HBB stops due to mass loss reducing the mass of the envelope, or because  ${}^3\text{He}$  is almost completely depleted in the envelope and  ${}^7\text{Li}$  is quickly destroyed by proton capture. It is thus expected that Li-rich TP-AGB stars appear in a limited luminosity domain which depends on the aforementioned factors (Forestini & Charbonnel 1997, Mazzitelli et al. 1999, Ventura et al. 2000, Travaglio et al. 2001, Karakas & Lugaro 2016, Ventura et al. 2018). The models are constrained by the observations of Li-rich TP-AGB stars in the Galaxy and in the Magellanic Clouds (Smith & Lambert 1989, 1990, Abia et al. 1991, Smith et al. 1995, García-Hernández et al. 2007).

The short duration of the Li-rich phase in TP-AGB stars has cast doubt on their ability to contribute significantly to  ${}^7\text{Li}$  enrichment on a galactic scale (Romano et al. 2001), in contrast to earlier expectations (Abia et al. 1993). The complexity of those phases, involving

---

**Hot Bottom Burning:** Stars with mass  $> 3\text{-}4 M_{\odot}$  develop very high temperatures ( $> 40$  MK) at the base of their deep convective envelopes, allowing for nuclear burning.

poorly understood mechanisms of mixing and mass loss, make the robust prediction of Li yields difficult (Cristallo & Vescovi 2020, Choplin et al. 2024). The predicted net Li yields of models with sub-solar metallicities are, in general, quite small or even negative, i.e., Li is destroyed rather than produced. Positive net yields are obtained in the calculations of Karakas & Lugaro (2016) for stars of twice solar metallicity (Fig. 7, left) and, interestingly, they are just at the level required by GCE models to produce most of the proto-solar Li. Taken at face value, the AGB yields of Karakas & Lugaro (2016) for metallicities up to solar fail to reproduce the proto-solar Li abundance by large factors. However, in view of the many uncertainties in the treatment of this complex phase of stellar nucleosynthesis it would be premature to exclude AGBs as an important Li source.

**Stellar Yield:** Total amount of a given element ejected by a star of a given mass.

**Net yield:** The difference between the ejected mass of an element and the one that originally entered the ejected part of the star.

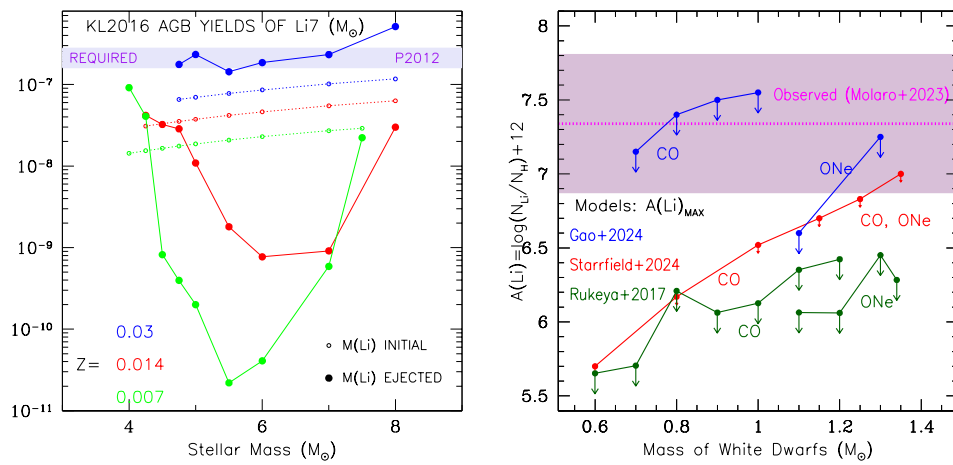


**Figure 7**

*Left:* AGB yields of Li from HBB in models of stars of  $4-8 M_{\odot}$  from Karakas & Lugaro (2016), for 3 initial metallicities. Ejected masses (solid lines) are lower than initial ones (dotted) and insufficient to produce proto-solar Li (as indicated by the shaded area, obtained through GCE models in Prantzos 2012), except for supersolar metallicity stars (blue solid).

*Right:* Relative abundances of Li in nova explosions. The shaded area shows the range of observed values and the red horizontal dotted line is the average value. Points connected by curves represent the highest values found in recent nova calculations; those of José et al. (2020) with 2-D models lie below the lower bound of the figure (adapted from Borisov et al. (2024b) and reference therein).

#### 4.4. Explosive H-burning in novae

In one of the earliest attempts to explain the nova phenomenon, a thermonuclear explosion of the H-layer at the surface of a white dwarf was invoked, triggered by  $^{3}\text{He} + ^{3}\text{He}$  (Schatzman 1951). Gurevitch & Lebedinsky (1957) suggested that a plausible trigger of novae would be reactions involving the unstable isotopes of N ( $^{13}\text{N}$ ) and O ( $^{14}\text{O}$  and  $^{15}\text{O}$ ) with the overall rate of the CNO cycle being determined by their beta-decay timescales, of the order of  $\sim 100$  s (the "beta limited hot CNO cycle"). This was confirmed quantitatively with a hydrodynamic code incorporating a nuclear reaction network by Starrfield et al. (1972).

The role of nova as potential producers of  $^{7}\text{Li}$  was revealed in Arnould & Norgaard (1975) who performed nucleosynthesis calculations of explosive H-burning with parametrized temperature and density profiles and noticed the importance of the initial amount of  $^{3}\text{He}$  on

the final  ${}^7\text{Li}$  abundance. Their results were confirmed with the hydro+nuclear code of Starrfield et al. (1978), who emphasized the impact of uncertainties of the nova modelling - in particular the speed and duration of convection - on the  ${}^7\text{Li}$  production. Subsequent observations and calculations refined the picture of nova eruptions over the years (see e.g. José 2017, for extensive reviews of nova properties and models). Regarding nucleosynthesis, there is general agreement that the main nucleosynthetic products are Li7, C13, N15, O17, all of them being formed with large overproduction factors of  $\sim 10^3$ .

For 40 years after the work of Arnould & Norgaard (1975) no observations of Li were reported in nova spectra. The line of Li I at 6708 Å in the early high-resolution spectra of the “slow” nova V1369 Cen was possibly detected by Izzo et al. (2015). The parent nucleus  ${}^7\text{Be}$  was detected with high-resolution spectrographs in several recent novae and also found in reanalysis of archival data of historical novae from the *International Ultraviolet Explorer* (Molaro et al. 2023, and references therein).

Nova observations show that Li/H is on average almost 10000 times higher than the proto-solar one (Fig. 7, right). This is in contrast with the predictions of almost all old and recent nova models (José & Hernanz 1998, Starrfield et al. 2016, Rukeya et al. 2017, Starrfield et al. 2024), which produce at least 10 times lower values. Unlike previous studies, the one of Gao et al. (2024) finds maximum  ${}^7\text{Be}$  abundances compatible with the observed ones, especially for CO novae. They attribute it to the high mass fraction of  ${}^3\text{He}$  assumed in their calculations combined to the treatment of element diffusion during the nova eruption. However, Denissenkov et al. (2021) found that a high abundance of  ${}^3\text{He}$  affects the energetics of the explosion (through the  ${}^3\text{He} + {}^3\text{He}$  reaction which ignites at lower temperature than  ${}^{12}\text{C} + \text{p}$ ), decreases the peak temperatures and accreted masses and results in a reduced production of  ${}^7\text{Be}$ .

Nova calculations are still affected from several poorly known physical ingredients (José 2017). Moreover, 1D models can hardly provide a realistic description of e.g. convection or the ignition of the explosion, which may occur in “hot-spots” and not simultaneously on the whole surface of the WD. Multidimensional hydro codes are definitely required for a more accurate description of the nova phenomenon. Despite the work of various groups for more than 30 years and the initially encouraging results regarding the core-envelope mixing, progress in that direction has been rather slow and contradictory results have been obtained sometimes (e.g. José 2017, and references therein). Using a multiD model José et al. (2020) find results similar to those obtained with 1D models for most nuclear species, except for  ${}^7\text{Be}$  for which considerably lower values are found.

Despite the disagreement between current nova models and observational findings on Li, observations support strongly the role of novae as the main stellar source of Li. The observationally inferred Li yields of novae<sup>5</sup>, combined to the currently observed Galactic nova rates and despite the poorly known nova history in the Galaxy, reproduce satisfactorily the protosolar Li abundance (see § 5.1).

#### 4.5. $\nu$ induced nucleosynthesis in core-collapse supernovae

In their seminal study on the hydrodynamical behaviour of supernovae, Colgate & White (1966) found that a) the large energy released by the gravitational collapse of the Fe core

---

<sup>5</sup>The nova Li yields are derived from observations of Li/H taking into account the total mass of the ejecta, since H in nova has a considerably lower abundance than in the Sun.

of a massive star ( $\sim 10^{53}$  ergs) would be mostly in the form of neutrinos emitted from the naissant proto-neutron star and that b) partial transfer of this energy to the stellar mantle could lead to a successful explosion.

Domogatsky & Nadyozhin (1977) suggested that in view of the huge number of the emitted neutrinos ( $\sim 10^{58}$ ) their interactions with the nuclei of the stellar envelope might have interesting nucleosynthetic effects, despite the extremely low values of the corresponding cross-sections which are  $\sim 10^{-45}$  cm<sup>2</sup>. Indeed, the energies of the neutrinos reflect the temperature of the proto-neutron star (several  $\sim 10^{11}$  K) and are in the range of tens of MeV, comparable to the excitation energies of nuclei. The excited nuclei decay through emission of photons, neutrons, protons, or  $\alpha$  particles (and in some cases, also deuterons or  $^3$ He) and these particles interact in their turn with their hot and dense environment during the passage of the shock wave (Domogatsky et al. 1978). Woosley et al. (1990) performed the first thorough investigation of the process, involving the evaluation of all relevant cross-sections and branching ratios and a simulation of the pre- and post-shock conditions in the various layers of a CCSN of  $20 M_{\odot}$ . Regarding the light nuclei, they found that substantial amounts of  $^7$ Li could be produced in the He-shell through  $^4$ He+ $^3$ He  $\rightarrow$   $^7$ Be and  $^4$ He+ $^3$ H  $\rightarrow$   $^7$ Li, with  $^3$ He and  $^3$ H produced by de-excitation of  $\nu$ -excited  $^4$ He; moreover, significant production of  $^{11}$ B could occur in the C-shell through de-excitation of  $\nu$ -excited  $^{12}$ C.

Subsequent studies, with improved stellar, supernova, nuclear and neutrino physics progressively refined that picture. Considering time-dependent spectra for all  $\nu$  species from supernova simulations (rather than a parametric description of  $\nu$ -luminosity from the neutron star cooling phase) and the neutrino emission from the initial neutrino burst and accretion phases, Sieverding et al. (2019) found that relevant amounts of  $^7$ Li can be produced in a  $27 M_{\odot}$  star (Fig. 5, bottom panel).

Neutrino-induced nucleosynthesis is a relatively recent and fascinating chapter regarding supernova explosions and the origin of the elements (see, e.g. Fischer et al. 2024, for a review). It offers a way to explain the proto-solar  $^{11}$ B/ $^{10}$ B ratio, but most probably it does not contribute to the production of Li in the Galaxy (§ 5.4).

## 5. LITHIUM AS A PROBE OF THE CHEMICAL AND DYNAMICAL EVOLUTION OF THE GALAXY

The evolution of Li was considered in some of the earliest models of Galactic Chemical Evolution (GCE thereafter) in the early 1970s (Mitler 1970, Reeves et al. 1973, Truran & Cameron 1971, Audouze & Tinsley 1974). However, its fragility makes such studies difficult on two grounds: on the theoretical side, because of the uncertainties affecting the Li yields of the major candidate stellar sources (§ 4) and the time dependence of their rates; and on the observational side, because the photospheric abundance of Li does not reflect, in general, the one at the star's formation (except for the hottest and youngest stars), thus preventing an unbiased comparison between model predictions and observations.

### 5.1. The solar vicinity and the main Li source

Most studies of Li evolution concern the solar vicinity (loosely defined as a cylinder of diameter  $\sim 1$  kpc perpendicular to the plane of the Galactic disk and centered on the Sun) and are made with simple 1-zone models. Such models produce a unique age-metallicity relation allowing for Fe to be used as a proxy for age, since stellar ages still suffer from

considerable uncertainties. Boundary conditions to such models are: a) the present-day Li abundance, b) the one at the Sun's formation (4.56 Gyr ago) c) the initial one (resulting from BBN) and d) the 'upper envelope' of the Li observations (hereafter ULiE).

a) The Li abundance is  $A(\text{Li})=3.25\pm0.15$  in the local ISM (Knauth et al. 2003), and similar values were obtained for young stars in Orion (Cunha et al. 1995, Kos et al. 2021) and in the young cluster NGC2664, estimated to be  $<5$  Myr old (Lim et al. 2016).

b) The proto-solar value, measured in meteorites, has been recently evaluated slightly upwards from previous ones, to  $A(\text{Li})_{\text{P}-\odot}=3.39\pm0.02$  (Lodders et al. 2025).

c) SBBN gives values of  $A(\text{Li})_{\text{SBBN}} \sim 2.70$  (§ 4.2), implying that the primordial contribution to the proto-solar Li abundance is  $\sim 20\%$ . A similar contribution comes from GCR (§ 4.1).

d) In the past the ULiE has been interpreted as a tracer of the true Li evolution (Rebolo et al. 1988), and it was used - incorrectly - to determine the timescale of the stellar Li source. However, the leading alternative interpretation (Lambert et al. 1991) is that "*the galactic Li abundance at a given [Fe/H] exceeds the observed maximum abundance and has been reduced in all stars to give the observed abundances*", i.e. the ULiE constitutes a lower limit constraining the true Li evolution from below.

The role of the various candidate Li sources has been scrutinized over the years (Audouze et al. 1983, D'Antona & Matteucci 1991, Abia et al. 1995, Matteucci et al. 1995, Romano et al. 2001, Travaglio et al. 2001, Prantzos 2012). Available Li yields of all stellar sources seemed insufficient to make the required amount of Li. In the past ten years novae attracted considerable attention, due to the detection of substantial abundances of  ${}^7\text{Be}$  in their ejecta (§ 4.4). One-zone GCE models using Li yields inferred from observed nova abundances now reproduce the meteoritic Li value (Rukeya et al. 2017, Cescutti & Molaro 2019, Grisoni et al. 2019, Romano et al. 2021, Kemp et al. 2022a, Gao et al. 2024, Borisov et al. 2024b, Nguyen et al. 2025). These models make different assumptions on the history of the nova rate, which is only constrained from its observed current Galactic value of  $\sim 30-50 \text{ yr}^{-1}$  (Shafter 2017, De et al. 2021, Kawash et al. 2022). It constitutes a critical ingredient of the models, non-trivially connected to the assumed star formation rate through the nova Delayed Time Distribution (DTD).

Various evaluations/approximations of the nova DTD have been proposed in the literature and adopted in the GCE models. The most complete study is the population synthesis of Kemp et al. (2022b) accounting for various factors on the evolution of binary systems (mass, initial separation and metallicity), which -interestingly - *predicts typical ejecta masses compatible with observed ones* and a strong dependence of the nova DTD on the metallicity of the progenitor system. Besides the metallicity dependence, a peculiar feature of that DTD (a power law as function of time) is that its slope  $X_{\text{NOV}}$  is systematically shallower - for all metallicities - than the corresponding one of SNIa ( $X_{\text{SNIa}} \sim -1$ ). The production ratio  $\text{Li}(\text{novae})/\text{Fe}(\text{SNIa})$  increases with time after a burst of star formation and particularly at late times<sup>6</sup>, with the characteristic timescales being of a several  $10^8 \text{ yr}$  for SNIa and  $>1 \text{ Gyr}$  for novae.

As a result, *for the same metallicity* a slowly evolving system reaches a higher Li abun-

**Upper Lithium Envelope (ULiE):**  
The highest Li abundance observed at a given metallicity, evaluated by taking the average of (a few of) the most Li-rich stars in that metallicity range.

**Delayed Time Distribution(DTD):**  
The frequency distribution in time of some stellar events (AGBs,novae, SNIa) after the formation episode of their progenitor sources

<sup>6</sup>In the case of SNIa, observations of external galaxies are used to evaluate reasonably well their  $\text{DTDSNIa} \propto \text{time}^{-1}$  but no such observations exist for novae. The production ratio  $\text{Li}(\text{novae})/\text{Fe}(\text{SNIa})$  varies with time  $t$  as  $t^{X_{\text{NOV}}}/t^{-1}=t^{(X_{\text{NOV}}+1)}$ , i.e. it increases with time for all values of  $X_{\text{NOV}} > -1$ , which is the case of the DTDs of Kemp et al. (2022a).

dance than a rapidly evolving one, because in the latter case, metallicity increases faster, in such short timescales that most long-lived sources - like novae - have no time to release their Li (Prantzos et al. 2017). The DTD of Li sources has important implications for the interpretation of the Li observations, both locally and Galaxy wide. A short-timescale source of Li breaks at earlier times and lower metallicities the primordial Li plateau than a long-lived one, but it leads to a smaller Li increase at late times and high metallicities. This feature explains most of the differences between GCE models of Li having novae as the main/only stellar source.

It should be emphasized that 1-zone models like the one in Fig. 8 (left panel), represent poorly the situation, either in the Galactic halo ( $[Fe/H] < -1$ ), or in the local disk. Indeed, the local super-solar metallicity stars were suggested to originate from the inner disk (Grenon 1989), and the large scatter in the local age-metallicity relation from diffusion of stars from other regions to the solar neighborhood (Edvardsson et al. 1993); we discuss those points, crucial for understanding Li evolution, in the next section. On the other hand, the halo is thought to be formed by an ensemble of smaller subhaloes with different histories and age-metallicity relations. However, the abundance ratios between primary elements having the same source (e.g. O and Mg, as well as Fe from CCSN) are expected to be constant as a function of time. The same holds for the GCR components of Li ( ${}^6\text{Li}$  and  ${}^7\text{Li}$ ) calculated as described in Prantzos (2012), in which case the evolution depicted in Fig. 8 (left) for the contribution of GCR can be considered “realistic” (see § 5.4 for alternatives).

---

**Primary elements:**

Elements with yields independent of the initial metal content of their parent star, like e.g. O or Fe from massive stars.

---

## 5.2. Evolution of Li in the Milky Way thin disk

An early attempt to extend the study of Li evolution from the solar vicinity to the whole Galactic disk was made in Prantzos (2012) with an independent-ring multi-zone model; adopting a long-lived stellar Li source, he predicted a present-day Li gradient of  $d[\text{Li}/\text{H}]/dR = -0.05 \text{ dex/kpc}$ , not very different from the one of oxygen. However, Sellwood & Binney (2002) revealed the importance of radial migration of stars for the evolution of galactic disks. Radial migration turns out to be crucial in interpreting Li observations in the Milky Way, even more so than for other, less fragile elements.

A first “alert” in that respect came from the unexpected finding of a non-monotonic behaviour of the ULiE, namely a decline of Li/H at super-solar metallicities (Delgado Mena et al. 2015, Guiglion et al. 2016, Fu et al. 2018, Bensby & Lind 2018), with different data samples<sup>7</sup>. The extensive investigation of Delgado Mena et al. (2015) revealed that other properties of the ULiE also vary in a non monotonic way with metallicity, going through an extremum at  $[Fe/H] \sim 0$  (age, mass, average  $T_{\text{eff}}$ ). Guiglion et al. (2019) suggested that during the several Gyr time of their migration from the inner disk to the solar vicinity, super-solar metallicity stars may have depleted their original (presumably super-solar) Li to the presently observed levels. Their suggestion was confirmed by the investigation of Minchev et al. (2019) who used mono-age populations from the HARPS survey and Dantas et al. (2022) who included stellar kinematics from GES data.

Several surveys in the past decade have increased considerably the size and the quality of the data samples regarding Li in the Galactic disks: HARPS (Delgado Mena et al. 2015),

---

<sup>7</sup>Prantzos et al. (2017) explored the idea of strong reduction of AGB yields of Li at such high metallicities, while acknowledging that it is not supported by the stellar nucleosynthesis models of Karakas & Lugaro (2016, see § 4.3); they suggested that strong Li depletion in the stellar envelopes may contribute to, or even be at the origin of, the effect.

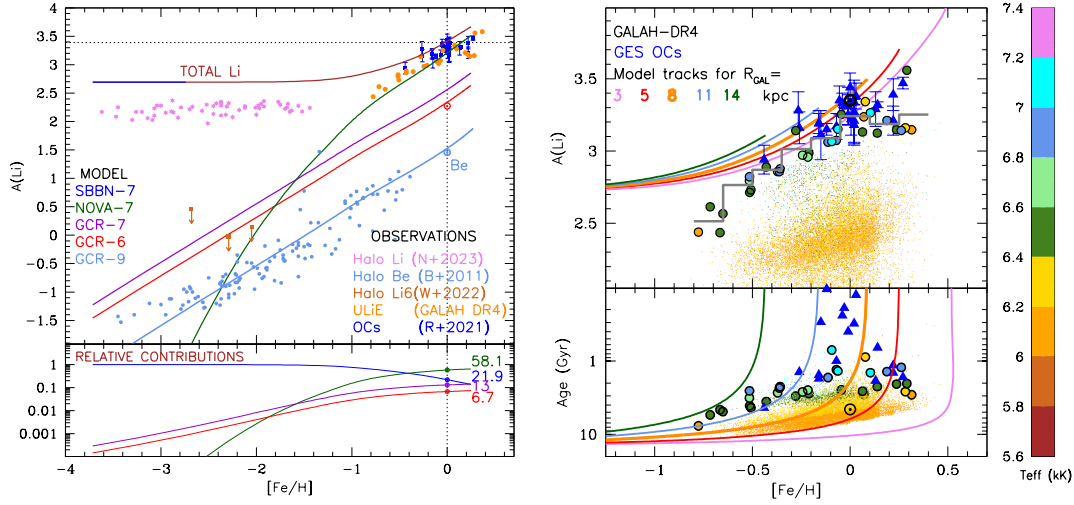


**Figure 8**

*Left top:* Evolution of Li and its components (BBN and novae for  $^7\text{Li}$  and GCR for  $^6\text{Li}$  and  $^7\text{Li}$ ) and of  $^9\text{Be}$  (a “monitor” of GCR activity and composition) as a function of  $[\text{Fe}/\text{H}]$  in a simple 1-zone model of the solar neighborhood (*top*). Data from Norris et al. (2023, for Li) with corrections applied in Borisov et al. (2024a), Boesgaard et al. (2011, for Be), Wang et al. (2022, for Li-6 upper limits with downward arrows), Romano et al. (2021, for Open Clusters) and Buder et al. (2025, GALAH DR4 Upper Li Envelope ULiE).

*Left bottom:* Contributions of individual components, with numbers indicating the corresponding percentage contributions at Sun’s formation.

*Right top:* a zoom on the upper right part of the top left figure, with field star data from GALAH DR4 in the solar neighborhood ( $7.5 < R_G/\text{kpc} < 8.5$ ), color coded for temperature with filled circles indicating the 4 most Li-rich stars in each  $[\text{Fe}/\text{H}]$  bin and the grey histogram indicating their average trend; blue triangles with error bars indicate OC data (no colour coding for temperature), while tracks of gas abundances of Li vs Fe in various galactocentric radii are from a multi-zone model of the Galaxy (Borisov et al. 2024b).

*Right bottom:* Corresponding stellar ages vs  $[\text{Fe}/\text{H}]$  with same colour-coding as in the top for the data and the model tracks.

AMBRE (Guiglion et al. 2016), LAMOST (Gao et al. 2019), GES (Randich et al. 2020, Romano et al. 2021), GALAH DR3 (Gao et al. 2020, Wang et al. 2024) and DR4 (Buder et al. 2025). The trend of declining Li/H was not confirmed by observations of stars hotter than the “Li-dip” in GES data of Open Clusters (OCs, Randich et al. 2020) and similar conclusions were reached by the analysis of GALAH DR3 data by Charbonnel et al. (2021) who discussed the potential impact of atomic diffusion on the Li abundances of those stars.

The aforementioned results are summarized in Fig. 8 (right) in terms of stellar temperatures and ages, using data from GES OCs and the GALAH DR4 field stars in the solar vicinity (Buder et al. 2025)<sup>8</sup>. At each metallicity bin, the ULiE is mainly formed by the hottest (top panel) and youngest (bottom panel) objects of that bin, the trend being essen-

<sup>8</sup>The GALAH DR4 stars used in Fig. 8 have  $\log g > 3.8$ , signal-to-noise ratio  $\text{SNR} > 80$ ,  $V\sin i < 20$  km/s. NLTE corrections (as found in Wang et al. 2024, for GALAH DR3 stars) have not been applied, but for hot stars they are insignificant (X. Wang, private communication).

tially monotonic with metallicity, except for the highest metallicities where it is reversed. The GALAH data concern a local stellar population, within less than a kpc from the Sun, but the large dispersion in their age-metallicity relation is a clear signature of stellar radial migration (bottom panel in Fig. 8, right, and Fig. 1S in Supplemental Material of the electronic edition).

The combined effects of stellar Li-depletion and radial migration render the use of [Fe/H] as a proxy for time obviously futile, even for stars found locally today. Therefore, the ULiE cannot be used to determine the timescale of the main stellar Li source as often done in the past. The locally observed ULiE is composed of stars formed in different places with different star formation histories and it is modulated by age and metallicity dependent Li depletion and radial migration (which determines the fraction of stars brought to the local volume from other radii). The timescale of radial migration ( $\sim 1$  kpc/Gyr), makes it statistically improbable - albeit not impossible - to find very young ( $< 1$  Gyr) and hot ( $> 6800$  K) stars of highly super-solar metallicity and very high Li values in the solar vicinity. The chances of finding such stars should increase with the size of the sample.

Similar results with those displayed in Fig. 8 (right), at least qualitatively, are obtained with the field stars of other surveys, like AMBRE (Guiglion et al. 2016) or GES (Romano et al. 2021). Moreover, GES provides data for OCs in a range of Galactocentric radii  $4 < R_G(\text{kpc}) < 14$ , thus offering important supplementary information. However, the effects of radial migration make it difficult to infer the present Li gradient from observations and to compare with models (see discussions in Romano et al. 2021, Borisov et al. 2024b).

Although the importance of radial migration in interpreting the Li observations has been properly emphasized in Minchev et al. (2019), a quantitative understanding of the impact of this effect is still lacking because of the difficulty of ‘unmixing’ the stellar populations of the disk. Attempts to determine the *birth radii* of stars for Li studies were made recently (Minchev et al. 2019, Zhang et al. 2023, Sun et al. 2025c, Dantas et al. 2025b), based on various stellar samples and methods. Methods dependent on GCE models and augmented by analysis of kinematic and dynamical data are recently developed in Dantas et al. (2025a). Methods independent of the GCE models, inferring the evolution of the Galactic metallicity gradient at birth radius from observations (Lu et al. 2024, Ratcliffe et al. 2023, 2024) are promising but not yet free from biases and rely on critical assumptions (Lu et al. 2022, Chen & Prantzos 2025). The application of a simple method, suggested in Minchev et al. (2018), is illustrated for the case of Li in Fig. 2S of the Supplemental material.

A quantitative assessment of the Li evolution in the Milky Way disk will require more elaborate, model independent, methods to determine the evolution of the metallicity gradient at birth place of stars. Such methods will need large and unbiased stellar samples with accurate age determinations, as well as dynamical and kinematic information from observations. Combining the chemodynamical evolution of the Galaxy to the study of Li in stars of various types, ages, metallicities, masses and rotational velocities will constitute a powerful probe of galactic and stellar evolution: the stellar age could be compared to the timescale of radial migration from its birthplace to the solar vicinity and to the timescale for its Li depletion expected from stellar models. It could thus constrain both those stellar and galactic physical effects, opening a new window for the study.

Despite the large number of stars with Li detection in current surveys, a much larger number of super-solar metallicity stars from the warm side of the Li dip will be necessary to assess the Li evolution in the  $[\text{Fe}/\text{H}] > 0.1$  region. Such large numbers will be needed for the training samples of machine learning techniques that could be used in the data analysis

of next generation spectroscopic surveys. The potential of Convolution Neural Networks to exploit large sets of Li data is illustrated in Nepal et al. (2023).

### 5.3. The evolution of Li in the thick disk and the bulge

Despite the large number of studies over the years, there is no clear identification of the thin and thick disks of the Galaxy, since their various properties (morphological, kinematic, chemical, stellar ages) overlap to various extents, the overlap depending on the galactic location (see e.g. Imig et al. 2023). Thus, the role played by the various processes invoked to explain the differences between those properties still remains unclear. An example is the observed double-branch behaviour of the  $[\alpha/\text{Fe}]$  ratio in the solar vicinity: high  $[\alpha/\text{Fe}]$  for the older thick disk and low  $[\alpha/\text{Fe}]$  for the younger thin disk at a given metallicity.

The behaviour of Li in the thick disk was investigated observationally in several studies (Molaro et al. 1997, Romano et al. 1999, Ramírez et al. 2012, Delgado Mena et al. 2015, Guiglion et al. 2016, Bensby & Lind 2018, Fu et al. 2018) who adopted different criteria for the definition of the thick disk (chemistry, kinematics, or age) and found different trends of Li/H vs [Fe/H], namely declining, increasing or constant.

The evolution of Li in the “low  $[\alpha/\text{Fe}]$ ” and “high  $[\alpha/\text{Fe}]$ ” disks was studied up to now with semi-analytical models, which can be classified in two categories: One class invokes models without radial migration, with two regimes of star formation in the MW (a fast and a slower one, occurring either sequentially or in parallel). They are separated by a pause in star formation during which the gaseous abundances at the end of the first regime are diluted by the infall of pristine material (Grisoni et al. 2019, Cescutti & Molaro 2019, Romano et al. 2021). The second class concerns multi-zone models with radial migration (Prantzos et al. 2017, Borisov et al. 2024b). The “high  $[\alpha/\text{Fe}]$ ” branch of the local population results from the presence of old ( $>9$  Gyr) migrant stars formed early on in the inner Galaxy while the “low  $[\alpha/\text{Fe}]$ ” branch is composed from stars formed locally or are migrants from the outer disk (at subsolar metallicities) or from the inner disk (at super-solar metallicities).

In all cases, the model evolution of Li in the gas of the high  $[\alpha/\text{Fe}]$  disk is determined mainly by the adopted pre-galactic abundance (SBBN vs Halo Plateau) and the timescale of the adopted Li stellar source. High pre-galactic abundances and/or long timescale sources produce a slow (or null) increase of Li in the gas of the high  $[\alpha/\text{Fe}]$  phase of the Galaxy (Prantzos et al. 2017, Cescutti & Molaro 2019, Grisoni et al. 2019). This is not necessarily reflected in the observed stellar Li abundances of the high  $[\alpha/\text{Fe}]$  disk which are affected by depletion to various extents and may lead to declining trends of Li/H vs metallicity (see Minchev et al. 2018, using monoage samples from AMBRE data). An understanding of the impact of the various stellar parameters on the amount of that depletion is required in order to decipher the early and late evolution of Li, as attempted in Nguyen et al. (2025).

Similar conclusions hold for the evolution of Li in the Galactic bulge, explored observationally by Bensby et al. (2020), who found a decline of Li/H at low metallicity, akin to the one of the thick disk. The existence of several stellar components in the bulge (Wylie et al. 2021) suggests a complex history for that region, involving stellar populations with different star formation histories. The interpretation of the Li abundances in the bulge would be at least as complex as the one for the solar neighborhood. A non-monotonic behaviour of Li/H with age or metallicity is expected, modulated by depletion.

## 5.4. The evolution of the ${}^6\text{Li}/{}^7\text{Li}$ ratio

Historically, the  ${}^6\text{Li}/{}^7\text{Li}$  ratio played an important role in studies of the light element evolution, because the lighter isotope has only one - and well understood - source, namely GCR. Thus, any important variation of that ratio between its meteoritic value and the one in the ISM would probe the differential activity between GCR and any stellar source of  ${}^7\text{Li}$  in the past 4.5 Gyr in the Galaxy (Reeves 1993). However, the situation becomes more complicated by the role of several factors, such as recent infall, presumably of primordial composition, which should dilute more  ${}^6\text{Li}$  than  ${}^7\text{Li}$  (since the former does not exist in primordial matter). Measurements of the  ${}^6\text{Li}/{}^7\text{Li}$  in the local ISM (Kawanomoto et al. 2009, Knauth et al. 2017) provide values compatible with the meteoritic one and with simple GCE models (Prantzos 2012). On the other hand, significantly higher values of  ${}^6\text{Li}/{}^7\text{Li}$  (factors 2-4) have been reported in several lines of sight to Galactic regions of stellar or supernova activity, like the SN remnant IC433 (Taylor et al. 2012) or the star forming region IC 348 (Knauth et al. 2017). This clearly argues for intense activity of energetic particles accelerated by local supernovae and disfavours any contribution of the  $\nu$ -process to  ${}^7\text{Li}$ . In contrast, the upper limit of  ${}^6\text{Li}/{}^7\text{Li} < 0.1$  obtained in the line of sight towards Sk 143 in the LMC (Molaro et al. 2024) is compatible with the meteoritic value.

---

**Secondary elements:**  
Their yields depend on the metallicity of their parent star (e.g. s- elements from AGB stars)

---

The behaviour of  ${}^6\text{Li}$  in halo stars was extensively investigated because it may provide information either about non-standard primordial nucleosynthesis or about the physics of GCR - spectra, energetics, composition, confinement - in the early Galaxy ,(Prantzos et al. 1993, Fields & Olive 1999, Ramaty et al. 2000, Prantzos 2006, 2012). Up to now, only upper limits on  ${}^6\text{Li}$  have been obtained (Lind et al. 2013, Wang et al. 2022). On the theoretical side,  ${}^6\text{Li}$  was expected to behave as a primary element at early times, its production been dominated by  $\alpha + \alpha$  fusion reactions (Steigman & Walker 1992). The underlying assumption is that GCR are accelerated from the ISM and therefore CNO spallation reactions produce always secondary Li, Be and B. However, observations of halo stars in the 1990s found an unexpected primary behaviour of Be (as depicted in Fig. 8, left). Prantzos (2012) suggested that GCR are accelerated in the winds of *rotating massive stars* always expelling primary CNO, in which case it is the spallation reactions of CNO that dominate the production of  ${}^6\text{Li}$  throughout the galactic history and not  $\alpha + \alpha$  fusion (see, however Tatischeff et al. 2021, for a different viewpoint on the acceleration site of GCR). In this oversimplified picture of LiBeB evolution,  ${}^6\text{Li}$  is expected to evolve in line with Be as primary, and its evolution is compatible with the current upper limits (see Fig. 8, top left), particularly if its nuclear fragility is taken into account. In contrast, using different assumptions about LiBeB production (a peculiar evolution of O/Fe and “overconfinement” of GCR in the early Galaxy) Fields & Olive (2022) find a considerably higher abundance of  ${}^6\text{Li}$ , which evolves as  $[\text{Fe}/\text{H}]^{0.5}$  (a kind of “overprimary”). They argue then that such a high theoretical abundance, compared to the current upper limits, implies a large destruction of  ${}^6\text{Li}$  and consequently of  ${}^7\text{Li}$ , independently of any models of Li destruction in stars. However,  ${}^6\text{Li}$  is destroyed  $\sim 100$  times faster than  ${}^7\text{Li}$  (Fig. 1, left) and its destruction should not constrain significantly the one of its heavier isotope.

In any case, the monitoring of the  ${}^6\text{Li}/{}^7\text{Li}$  ratio in early or late galactic environments can provide extremely useful information on various physical processes, in particular regarding the cosmic ray activity in comparison to the one of the stellar source of  ${}^7\text{Li}$ .

## SUMMARY POINTS

1. Compared to seismic solar-analogue stars, the Sun has a normal photospheric Li abundance and rotation rate at its present age.
2. The Li dip is a universal main sequence Li depletion phenomenon confined to the same effective temperature range for all metallicities at which it is potentially observable (i.e., down to  $[\text{Fe}/\text{H}] \sim -1$ ). All the evidence suggests that rotation-induced mixing is responsible for this pattern when stellar winds efficiently extract angular momentum early on the main sequence.
3. The universality of the Pop II Li plateau for  $[\text{Fe}/\text{H}]$  lower than  $\sim -1.0$  in the Milky Way and other galaxies implies that this feature does not result from the abstraction of a large fraction of the interstellar medium (ISM) of galactic haloes before the formation of Pop II stars. Instead, the discrepancy between the Li value predicted by BBN+CMB and the one observed along the Spite plateau has a stellar solution.
4. Type II rotating models including the transport of angular momentum and chemicals by meridional circulation and shear turbulence with specific prescriptions, together with a simple modelling of internal gravity waves, can simultaneously account for the Li abundance patterns in Pop I and II dwarf stars, including the solar Li, the Li dip, and the Spite plateau.
5. Thermohaline instability is currently favoured as the mechanism that can consistently explain the drops in lithium abundance, carbon isotopic ratio, and C/N ratio at the luminosity of the RGB bump.
6. When accounting for realistic stellar mass distribution in samples of red giants observed by large spectroscopic surveys together with a proper mass-dependent Li depletion on the MS, there is no evidence of an unknown Li production mechanism occurring between the upper RGB and the clump or the horizontal branch.
7. The proto-solar Li - meteoritic value  $A(\text{Li})=3.39$  results from a mixture of nucleosynthesis products of 3 different sites: early universe ( $\sim 20\%$ ), Galactic Cosmic rays ( $\sim 20\%$ ) and stars ( $\sim 60\%$ ). On observational grounds, novae are currently favoured as the main/only stellar source.
8. The evolutionary history of Li is poorly understood theoretically (in view of uncertainties in the Delay Time Distribution of novae) and hard to constrain observationally (because of depletion effects, depending on various stellar properties). The ULiE does not represent the evolutionary history of Li, it only constrains it providing lower values.
9. Stellar radial migration is a key to decipher the ULiE and, more generally, the observations of Li in the local volume and the disk of the Galaxy. Most of the super-solar metallicity stars observed locally are “messengers” from the inner disk and sub-solar metallicity ones from the outer disk, i.e., they probe regions with different star formation and Li histories.

## FUTURE ISSUES

1. The Li-age-mass- $T_{\text{eff}}$ - $[\text{Fe}/\text{H}]$  relations among different populations of stars derived from present and future surveys must be meticulously scrutinised through the mod-

elling of individual frequencies (to get the stellar mass, radius, age), combined with exquisite spectroscopic (to get the stellar effective temperature, metallicity, Li), photometric (to get  $P_{rot}$ ), and astrometric (to get the stellar luminosity) data, together with careful examination of the bias of the observed samples.

2. Li abundance in extremely metal-poor dwarfs with  $T_{eff}$  above  $\sim 6000$  K and no significant C-enrichment should lie on the Li plateau. Although such objects should be rare, they are worth searching for.
3. The measurement of the rotation of the deep solar core below  $0.2 R_{\odot}$  is required to legitimate the origin of the angular momentum transport process in the Sun and low-mass stars and its impact on the transport of chemicals that drives Li depletion.
4. The major limitations of the stellar evolution models come from the lack of understanding on shear turbulence, magnetic and hydrodynamic instabilities, and their interactions with (magneto)-gravito-inertial waves. There is an imperative need for extended formalisms that can self-consistently account for these mechanisms in stellar evolution models.
5. Important asteroseismic efforts must be devoted to ascertain the mass and the position in the HRD diagram of super Li-rich giant candidates.
6. A better understanding of Li production in nova (with extra ingredients or full 3D models) will be required to firmly establish their importance as main stellar Li producers. The same holds for the nova DTD.
7. Radial migration opens a new chapter in Li studies, which should rather be made on a star-by-star basis, combining the stellar properties and corresponding stellar depletion models with Galactic properties and chemo-dynamical models. The two aspects, stellar and galactic, are linked by the stellar ages for which a more accurate evaluation is required.
8. The field will benefit from next generation spectroscopic surveys (4MOST, WEAVE, 4MIDABLE). A much larger number of super-solar metallicity stars from the warm side of the Li dip will be necessary to explore the Li evolution in that extreme metallicity region.

## DISCLOSURE STATEMENT

The authors are not aware of any affiliations, memberships, funding, or financial holdings that might be perceived as affecting the objectivity of this review.

## ACKNOWLEDGMENTS

We are grateful to our colleagues who read and commented different sections of the manuscript, namely, L. Amard, S. Borisov, K. Cunha, J. José, N. Lagarde, I. Minchev, P. Molaro, A. Palacios, O. Richard, and S. Vauclair. We thank E. Wang for advice on GALAH DR4 Li data, and S. Randich and E. Franciosini for advice on GES data. We are grateful to S. Borisov for his kind help with the data management. CC acknowledges support from the Swiss National Science Foundation (SNF; Project 200021-212160, PI CC) and IAP for their hospitality during the writing of this review.

**SUPPLEMENTAL MATERIAL to Sec. 5.2: Evolution of Li in the Milky Way thin disk. Included only in the electronic edition of ARAA**

The same models and GALAH data as in Fig. 8 (right) of the Main Text (hereafter MT) are plotted as a function of age in Fig. 9 of the Supplemental Material (hereafter SM). Independently of the model tracks, observations suggest that the stars of the ULiE (the most Li-rich stars in the metallicity bins of Fig. 8) trace also an upper envelope for a given age (bottom panel of Fig. 9). However, the subsolar metallicity stars of the ULiE are, rather counterintuitively, systematically among the most metal-poor ones at a given age (see top panel of Fig. 9). The reason is that metal-poor stars have lower opacities, are hotter and have less extended envelopes than metal-rich stars of the same age; as a result, they deplete less their Li than their cooler counterparts. Indeed, a gradient of  $T_{\text{eff}}$  from cooler to hotter stars is observed in the metallicity vs age panel (top panel in Fig. 1) but an inverse gradient, from hotter to cooler stars, is observed in the lithium abundance vs age panel (bottom). Thus, at a given age, the hottest stars of sub-solar metallicities are the most metal-poor ones and preserve better their Li. In view of the observed negative Galactic metallicity gradient, those stars which compose the sub-solar metallicity ULiE, are logically formed in the outer disk. *Thus, observations of  $[\text{Fe}/\text{H}]$  and Li vs age in local stars, combined to our understanding of the metallicity impact on the physics of stellar envelopes, provide another strong argument for radial migration.*

This confirms the conclusions of Sec. 5.2 (MT), namely that abundance patterns of Li observed in the solar vicinity result from a complex interplay between stellar ages, metallicities and radial displacements (with other factors, like mass and rotation also playing a role). The ULiE for  $[\text{Fe}/\text{H}] < -0.1$  is composed of stars aged from a few to several Gyr from the outer disk brought in the solar vicinity by radial migration. Stars older than  $\sim 8-9$  Gyr and even lower  $[\text{Fe}/\text{H}]$  were formed instead in the inner disk, since the inside-out formation of the disk produces very few stars in the solar vicinity at such early times. As for the super-solar metallicity stars of GALAH and OCs (less than 2 Gyr old) which are presumably formed in the inner disk (see Sec. 5.2 in MT), it is at present unknown whether they suffered some Li depletion and by how much, because the theoretical predictions depend on the DTD of the main stellar source.

Minchev et al. (2019) were the first to emphasize that “... *the study of the production/destruction of lithium as function of birth radius will provide stronger constraints on chemical evolution models*”, not only regarding the super-solar but also the sub-solar metallicity regime. However, the effects of radial migration make it difficult to infer the present Li gradient from observations and to compare with models. Attempts to determine the *birth radii* of stars for Li studies were made recently : Zhang et al. (2023) evaluated birth radii  $R_B$  of stars using the simple prescription of Minchev et al. (2018) for the evolution of the Galactic gas metallicity gradient over time. Sun et al. (2025c) used GALAH DR3 data combined to ages derived from *Gaia* and adopted the method of Lu et al. (2024) to derive the birthplaces of the sample stars, while Dantas et al. (2025b) derive  $R_B$  by comparing positions of observed stars in the  $(R_G, [\text{Fe}/\text{H}])$  plane to results of the GCE model of Magrini et al. (2009), a model-dependent method.

The application of a simple method, suggested in Minchev et al. (2018), is illustrated in Fig. 10 for the GALAH DR4 stars of the ULiE: stars observed locally originate from the inner or the outer disk, in birth places depending on their age and metallicity (upper panel); their Li abundance today is lower than the one predicted from the GCE model at their inferred birth radius and the time of their birth (lower panel). This figure merely

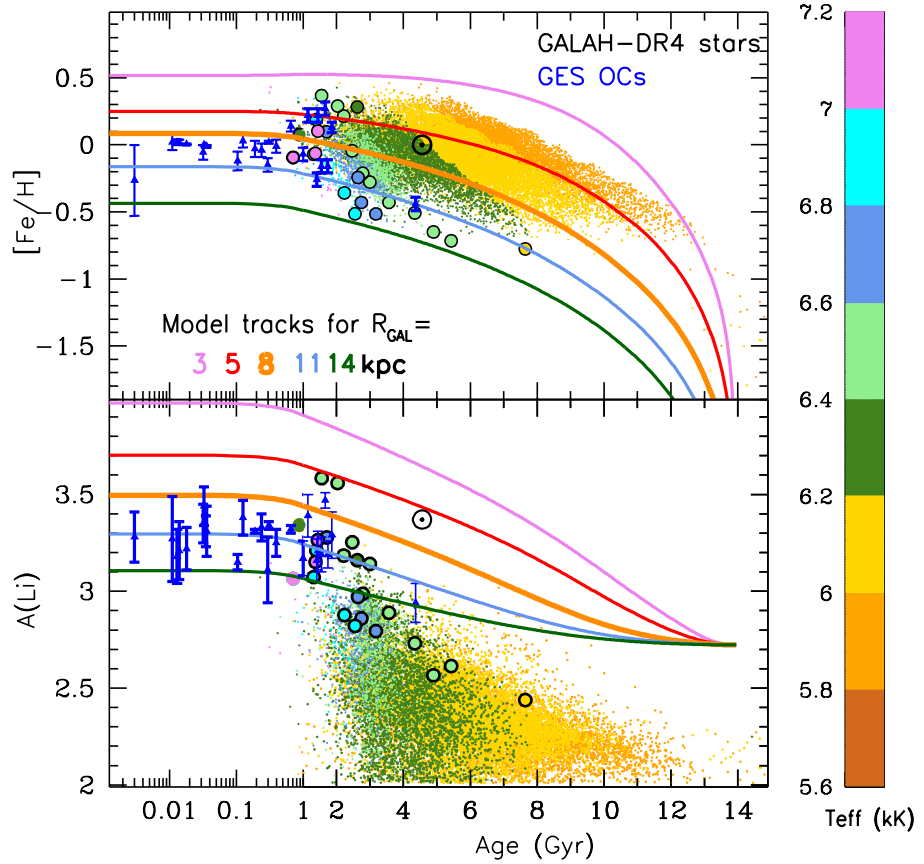


**Figure 9**

Same data, model tracks and color coding as in the right panels of Fig. 8, for GALAH DR4 local stars and GES OCs, plotted as function of age for  $[\text{Fe}/\text{H}]$  (top) and Li (bottom); the sub-solar metallicity stars of the ULiE are, in general, the metal-poorest ones (top panel) in each age bin, except for the case of the youngest ones (1-2 Gyr) which may have both sub-solar and super-solar metallicities..

illustrates the principle and the potential of the method, since the results obviously depend on the adopted GCE model (including the nova Delayed Time Distribution) and on the selection biases affecting the ULiE of the GALAH DR4 sample.

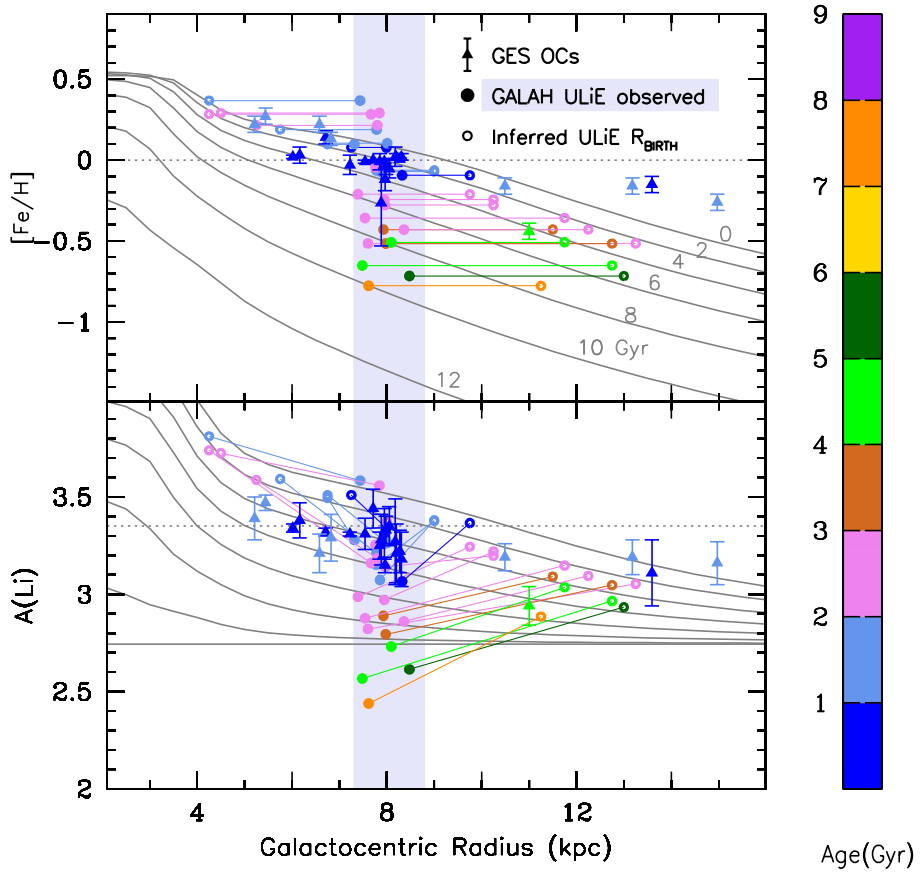


**Figure 10**

GES OC data (Romano et al. 2021, triangles with error bars) vs Galactocentric radius. Field stars of the GALAH DR4 ULiE, observed in the region of  $R_{\text{GAL}} = 7.5\text{--}8.5$  kpc, are plotted within the shaded area (filled circles). OCs and field stars are colour-coded with age. The stars - but not the OCs - are "projected" (top panel) into their birth radius (open symbols connected to the filled circles) by assuming that the  $[\text{Fe}/\text{H}]$ -metallicity relation in the Galaxy is well reproduced at every radius by the GCE model of Prantzos et al. (2023), as represented by the iso-age curves (in grey, labeled with the corresponding ages). The Li abundances of the model (calculated in Borisov et al. 2024b) at the inferred stellar birth places of the top panel are then connected to the locally observed ones in the bottom panel. While the Fe abundance is assumed to suffer no depletion, Li is obviously depleted during migration to the local volume, either from the inner or the outer disk.

## LITERATURE CITED

Abia C, Boffin HMJ, Isern J, Rebolo R. 1991. *A&A* 245:L1  
 Abia C, Isern J, Canal R. 1993. *A&A* 275:96–100  
 Abia C, Isern J, Canal R. 1995. *A&A* 298:465  
 Aerts C. 2021. *Reviews of Modern Physics* 93(1):015001  
 Aerts C, Mathis S, Rogers TM. 2019. *Ann. Rev. Astron. & Astrophys.* 57:35–78

Aguado DS, González Hernández JI, Allende Prieto C, Rebolo R. 2019. *ApJL* 874(2):L21

Aguado DS, Myeong GC, Belokurov V, Evans NW, Koposov SE, et al. 2021. *MNRAS* 500(1):889–910

Aguilera-Gómez C, Chanamé J, Pinsonneault MH, Carlberg JK. 2016. *ApJL* 833(2):L24

Aguilera-Gómez C, Jones MI, Chanamé J. 2023. *A&A* 670:A73

Alschuler WR. 1975. *ApJ* 195:649–660

Alvan L, Brun AS, Mathis S. 2014. *A&A* 565:A42

Alvan L, Mathis S, Decressin T. 2013. *A&A* 553:A86

Andersen BN. 1994. *Solar Physics* 152(1):241–246

Angelou GC, D’Orazi V, Constantino TN, Church RP, Stancliffe RJ, Lattanzio JC. 2015. *MNRAS* 450(3):2423–2440

Anthony-Twarog BJ, Deliyannis CP, Rich E, Twarog BA. 2013. *ApJL* 767(1):L19

Anthony-Twarog BJ, Deliyannis CP, Twarog BA, Croxall KV, Cummings JD. 2009. *AJ* 138(4):1171–1191

Anthony-Twarog BJ, Lee-Brown DB, Deliyannis CP, Twarog BA. 2018. *AJ* 155(3):138

Aoki M, Primas F, Pasquini L, Weiss A, Salaris M, Carollo D. 2021. *A&A* 653:A13

Arnould M, Norgaard H. 1975. *A&A* 42:55

Audouze J, Boulade O, Malinie G, Poilane Y. 1983. *A&A* 127(1):164–168

Audouze J, Tinsley BM. 1974. *ApJ* 192:487–500

Balachandran S. 1990. *ApJ* 354:310

Balachandran S. 1995. *ApJ* 446:203

Balachandran SC, Fekel FC, Henry GW, Uitenbroek H. 2000. *ApJ* 542(2):978–988

Balser DS, Wenger TV, Bania TM. 2022. *ApJ* 936(2):168

Barker AJ, Ogilvie GI. 2010. *MNRAS* 404(4):1849–1868

Barnes G, Charbonneau P, MacGregor KB. 1999. *ApJ* 511(1):466–480

Beck PG, do Nascimento Jr. JD, Duarte T, Salabert D, Tkachenko A, et al. 2017. *A&A* 602:A63

Bedding TR, Mosser B, Huber D, Montalbán J, Beck P, et al. 2011. *Nature* 471(7340):608–611

Benomar O, Bazot M, Nielsen MB, Gizon L, Sekii T, et al. 2018. *Science* 361(6408):1231–1234

Benomar O, Takata M, Shibahashi H, Ceillier T, García RA. 2015. *MNRAS* 452(3):2654–2674

Bensby T, Feltzing S, Yee JC, Johnson JA, Gould A, et al. 2020. *A&A* 634:A130

Bensby T, Lind K. 2018. *A&A* 615:A151

Bernas R, Gradsztajn E, Reeves H, Schatzman E. 1967. *Annals of Physics* 44(3):426–478

Bertulani CA, Hall FW, Santoyo BI. 2023. *Big Bang nucleosynthesis as a probe of new physics*. In *European Physical Journal Web of Conferences*, vol. 275 of *European Physical Journal Web of Conferences*

Bessila L, Mathis S. 2024. *A&A* 690:A270

Bessila L, Mathis S. 2025. *arXiv e-prints* :arXiv:2505.14650

Bethe HA. 1939. *Physical Review* 55(5):434–456

Böcek Topcu G, Afşar M, Schaeuble M, Sneden C. 2015. *MNRAS* 446(4):3562–3578

Boesgaard AM. 1987. *PASP* 99:1067–1070

Boesgaard AM. 2023. *ApJ* 943(1):40

Boesgaard AM, Armengaud E, King JR. 2003. *ApJ* 582(1):410–419

Boesgaard AM, Deliyannis CP. 2024. *ApJ* 972(2):136

Boesgaard AM, Lum MG, Chontos A, Deliyannis CP. 2022. *ApJ* 927(1):118

Boesgaard AM, Lum MG, Deliyannis CP, King JR, Pinsonneault MH, Somers G. 2016. *ApJ* 830(1):49

Boesgaard AM, Rich JA, Levesque EM, Bowler BP. 2011. *ApJ* 743(2):140

Boesgaard AM, Tripicco MJ. 1986. *ApJL* 302:L49

Bonifacio P, Caffau E, François P, Spite M. 2025. *A&A Review* 33(1):2

Bonifacio P, Caffau E, Spite M, Limongi M, Chieffi A, et al. 2015. *A&A* 579:A28

Bonifacio P, Molaro P. 1997. *MNRAS* 285(4):847–861

Bonifacio P, Sbordone L, Caffau E, Ludwig HG, Spite M, et al. 2012. *A&A* 542:A87

Borisov S, Charbonnel C, Prantzos N, Dumont T, Palacios A. 2024a. *A&A* 690:A245

Borisov S, Prantzos N, Charbonnel C. 2024b. *A&A* 691:A142

Bouvier J, Barrado D, Moraux E, Stauffer J, Rebull L, et al. 2018. *A&A* 613:A63

Bradt HL, Peters B. 1950. *Physical Review* 80(6):943–953

Braithwaite J, Spruit HC. 2017. *Royal Society Open Science* 4(2):160271

Brown JA, Sneden C, Lambert DL, Dutchover Jr. E. 1989. *ApJ Suppl. Series* 71:293

Brown JM, Garaud P, Stellmach S. 2013. *ApJ* 768(1):34

Buder S, Kos J, Wang XE, McKenzie M, Howell M, et al. 2025. *PASA* 42:e051

Buder S, Sharma S, Kos J, Amarsi AM, Nordlander T, et al. 2021. *MNRAS* 506(1):150–201

Buldgen G, Fellay L, Bétrisey J, Deheuvels S, Farnir M, Farrell E. 2024. *A&A* 689:A307

Buldgen G, Noels A, Amarsi AM, Nandal D, Pezzotti C, et al. 2025. *A&A* 694:A285

Burbidge EM, Burbidge GR, Fowler WA, Hoyle F. 1957. *Reviews of Modern Physics* 29(4):547–650

Burkhart C, Coupry MF. 1989. *A&A* 220:197–205

Burkhart C, Coupry MF. 2000. *A&A* 354:216–228

Caffau E, Bonifacio P, François P, Sbordone L, Monaco L, et al. 2011. *Nature* 477(7362):67–69

Cai B, Kong X, Shi J, Gao Q, Bu Y, Yi Z. 2023. *AJ* 165(2):52

Cameron AGW. 1955. *ApJ* 121:144

Cameron AGW, Fowler WA. 1971. *ApJ* 164:111

Cantiello M, Mankovich C, Bildsten L, Christensen-Dalsgaard J, Paxton B. 2014. *ApJ* 788(1):93

Canto Martins BL, Lèbre A, Palacios A, de Laverny P, Richard O, et al. 2011. *A&A* 527:A94

Carlos M, Meléndez J, do Nascimento JD, Castro M. 2020. *MNRAS* 492(1):245–249

Casali G, Montalbán J, Miglio A, Casagrande L, Magrini L, et al. 2025. *MNRAS* 541(3):2631–2650

Casey AR, Ruchti G, Masseron T, Randich S, Gilmore G, et al. 2016. *MNRAS* 461(3):3336–3352

Castro M, Baudin F, Benomar O, Samadi R, Morel T, et al. 2021. *MNRAS* 505(2):2151–2158

Castro M, Duarte T, Pace G, do Nascimento JD. 2016. *A&A* 590:A94

Cayrel R, Cayrel de Strobel G, Campbell B, Dappen W. 1984. *ApJ* 283:205–208

Cescutti G, Molaro P. 2019. *MNRAS* 482(4):4372–4382

Chaboyer B, Demarque P, Pinsonneault MH. 1995. *ApJ* 441:865

Chaboyer B, Zahn JP. 1992. *A&A* 253:173–177

Chanamé J, Pinsonneault MH, Aguilera-Gómez C, Zinn JC. 2022. *ApJ* 933(1):58

Chaplin WJ, Basu S, Huber D, Serenelli A, Casagrande L, et al. 2014. *ApJ Suppl. Series* 210(1):1

Charbonneau P, MacGregor KB. 1993. *ApJ* 417:762

Charbonnel C. 1994. *A&A* 282:811–820

Charbonnel C, Balachandran SC. 2000. *A&A* 359:563–572

Charbonnel C, Borisov S, de Laverny P, Prantzos N. 2021. *A&A* 649:L10

Charbonnel C, Brown JA, Wallerstein G. 1998. *A&A* 332:204–214

Charbonnel C, Lagarde N. 2010. *A&A* 522:A10

Charbonnel C, Lagarde N, Jasniewicz G, North PL, Shetrone M, et al. 2020. *A&A* 633:A34

Charbonnel C, Primas F. 2005. *A&A* 442(3):961–992

Charbonnel C, Talon S. 1999. *A&A* 351:635–643

Charbonnel C, Talon S. 2005a. *Science* 309(5744):2189–2191

Charbonnel C, Talon S. 2005b. *New generation stellar models with rotation and internal gravity waves: The Li dip revisited*. In *EAS Publications Series*, eds. G Alecian, O Richard, S Vauclair, vol. 17 of *EAS Publications Series*

Charbonnel C, Zahn JP. 2007. *A&A* 467(1):L15–L18

Chen T, Prantzos N. 2025. *A&A* 694:A120

Choplin A, Siess L, Goriely S, Martinet S. 2024. *Galaxies* 12(5):66

Christensen-Dalsgaard J. 2021. *Living Reviews in Solar Physics* 18(1):2

Coelho HR, Miglio A, Morel T, Lagarde N, Bossini D, et al. 2024. *MNRAS* 527(3):8535–8550

Colgate SA, White RH. 1966. *ApJ* 143:626

Cooke R. 2024. *arXiv e-prints* :arXiv:2409.06015

Cristallo S, Vescovi D. 2020. *Memorie della Societa Astronomica Italiana* 91:67

Cummings AC, Stone EC, Heikkila BC, Lal N, Webber WR, et al. 2016. *ApJ* 831(1):18

Cummings JD, Deliyannis CP, Anthony-Twarog B, Twarog B, Maderak RM. 2012. *AJ* 144(5):137

Cummings JD, Deliyannis CP, Maderak RM, Steinhauer A. 2017. *AJ* 153(3):128

Cunha K, Smith VV, Lambert DL. 1995. *ApJ* 452:634

Dantas MLL, Guiglion G, Smiljanic R, Romano D, Magrini L, et al. 2022. *A&A* 668:L7

Dantas MLL, Smiljanic R, de Souza RS, Tissera PB, Magrini L. 2025a. *A&A* 696:A205

Dantas MLL, Smiljanic R, Romano D, Guiglion G, Magrini L, et al. 2025b. *arXiv e-prints* :arXiv:2505.17173

D'Antona F, Matteucci F. 1991. *A&A* 248:62

De K, Kasliwal MM, Hankins MJ, Sokoloski JL, Adams SM, et al. 2021. *ApJ* 912(1):19

Deal M, Goupil MJ, Marques JP, Reese DR, Lebreton Y. 2020. *A&A* 633:A23

Deheuvels S, Ballot J, Eggenberger P, Spada F, Noll A, den Hartogh JW. 2020. *A&A* 641:A117

Deheuvels S, Doğan G, Goupil MJ, Appourchaux T, Benomar O, et al. 2014. *A&A* 564:A27

Delgado Mena E, Bertrán de Lis S, Adibekyan VZ, Sousa SG, Figueira P, et al. 2015. *A&A* 576:A69

Delgado Mena E, Tsantaki M, Sousa SG, Kunitomo M, Adibekyan V, et al. 2016. *A&A* 587:A66

Deliyannis CP, Anthony-Twarog BJ, Lee-Brown DB, Twarog BA. 2019. *AJ* 158(4):163

Deliyannis CP, Demarque P, Kawaler SD. 1990. *ApJ Suppl. Series* 73:21

Deliyannis CP, Pinsonneault MH, Charbonnel C. 2000. *Sinks of Light Elements in Stars - Part I (Invited Paper)*. In *The Light Elements and their Evolution*, eds. L da Silva, R de Medeiros, M Spite, vol. 198 of *IAU Symposium*

Denissenkov PA. 2010. *ApJ* 723(1):563–579

Denissenkov PA, Merryfield WJ. 2011. *ApJL* 727(1):L8

Denissenkov PA, Pinsonneault M, MacGregor KB. 2009. *ApJ* 696(2):1823–1833

Denissenkov PA, Ruiz C, Upadhyayula S, Herwig F. 2021. *MNRAS* 501(1):L33–L37

Di Mauro MP, Ventura R, Cardini D, Stello D, Christensen-Dalsgaard J, et al. 2016. *ApJ* 817(1):65

Ding MY, Shi JR, Yan HI, Li CQ, Gao Q, et al. 2024. *ApJ Suppl. Series* 271(2):58

Dintrans B, Brandenburg A, Nordlund Å, Stein RF. 2005. *A&A* 438(1):365–376

Dintrans B, Rieutord M, Valdettaro L. 1999. *Journal of Fluid Mechanics* 398:271–297

do Nascimento Jr. JD, Charbonnel C, Lèbre A, de Laverny P, De Medeiros JR. 2000. *A&A* 357:931–937

do Nascimento Jr. JD, Takeda Y, Meléndez J, da Costa JS, Porto de Mello GF, Castro M. 2013. *ApJL* 771(2):L31

Domogatsky GV, Eramzhian RA, Nadezhin DK. 1978. *Astroph. & Space Science* 58(2):273–299

Domogatsky GV, Nadyozhin DK. 1977. *MNRAS* 178:33P–36P

Dumont T. 2023. *A&A* 677:A119

Dumont T, Charbonnel C, Palacios A, Borisov S. 2021a. *A&A* 654:A46

Dumont T, Palacios A, Charbonnel C, Richard O, Amard L, et al. 2021b. *A&A* 646:A48

Edvardsson B, Andersen J, Gustafsson B, Lambert DL, Nissen PE, Tomkin J. 1993. *A&A* 275:101

Eggenberger P, Maeder A, Meynet G. 2005. *A&A* 440(1):L9–L12

Eggenberger P, Moyano FD, den Hartogh JW. 2022. *A&A* 664:L16

Fields BD, Olive KA. 1999. *ApJ* 516(2):797–810

Fields BD, Olive KA. 2022. *Journal of Cosmology & Astroparticle physics* 2022(10):078

Fields BD, Olive KA, Yeh TH, Young C. 2020. *Journal of Cosmology & Astroparticle physics* 2020(3):010

Fischer T, Guo G, Langanke K, Martínez-Pinedo G, Qian YZ, Wu MR. 2024. *Progress in Particle and Nuclear Physics* 137:104107

Forestini M, Charbonnel C. 1997. *A&A Suppl. Ser.* 123:241–272

Fowler WA, Burbidge GR, Burbidge EM. 1955. *ApJ Suppl. Series* 2:167

François P, Pasquini L, Biazzo K, Bonifacio P, Palsa R. 2013. *A&A* 552:A136

Fraser AE, Reifenstein SA, Garaud P. 2024. *ApJ* 964(2):184

Frebel A, Collet R, Eriksson K, Christlieb N, Aoki W. 2008. *ApJ* 684(1):588–602

Frebel A, Ji AP, Ezzeddine R, Hansen TT, Chiti A, et al. 2019. *ApJ* 871(2):146

Fu X, Romano D, Bragaglia A, Mucciarelli A, Lind K, et al. 2018. *A&A* 610:A38

Fuller J, Lecoanet D, Cantiello M, Brown B. 2014. *ApJ* 796(1):17

Fuller J, Piro AL, Jermyn AS. 2019. *MNRAS* 485(3):3661–3680

Gao J, Zhu C, Lü G, Yu J, Li L, et al. 2024. *ApJ* 971(1):4

Gao Q, Shi JR, Yan HL, Yan TS, Xiang MS, et al. 2019. *ApJ Suppl. Series* 245(2):33

Gao X, Lind K, Amarsi AM, Buder S, Bland-Hawthorn J, et al. 2020. *MNRAS* 497(1):L30–L34

Garaud P, Gagnier D, Verhoeven J. 2017. *ApJ* 837(2):133

Garcia RA, Turck-Chièze S, Jiménez-Reyes SJ, Ballot J, Pallé PL, et al. 2007. *Science* 316(5831):1591

García-Hernández DA, García-Lario P, Plez B, Manchado A, D’Antona F, et al. 2007. *A&A* 462(2):711–730

Garcia Lopez RJ, Rebolo R, Herrero A, Beckman JE. 1993. *ApJ* 412:173

Garcia Lopez RJ, Spruit HC. 1991. *ApJ* 377:268

Gehan C, Mosser B, Michel E, Samadi R, Kallinger T. 2018. *A&A* 616:A24

Gieles M, Padoan P, Charbonnel C, Vink JS, Ramírez-Galeano L. 2025. *MNRAS*

Gilroy KK. 1989. *ApJ* 347:835

Gough DO, McIntyre ME. 1998. *Nature* 394(6695):755–757

Gratton RG, Sneden C, Carretta E, Bragaglia A. 2000. *A&A* 354:169–187

Greenstein JL, Richardson RS. 1951. *ApJ* 113:536

Greenstein JL, Tandberg Hanssen E. 1954. *ApJ* 119:113

Grenon M. 1989. *Astroph. & Space Science* 156(1-2):29–37

Grisoni V, Matteucci F, Romano D, Fu X. 2019. *MNRAS* 489(3):3539–3546

Gruyters P, Lind K, Richard O, Grundahl F, Asplund M, et al. 2016. *A&A* 589:A61

Guiglion G, Chiappini C, Romano D, Matteucci F, Anders F, et al. 2019. *A&A* 623:A99

Guiglion G, de Laverny P, Recio-Blanco A, Worley CC, De Pascale M, et al. 2016. *A&A* 595:A18

Gurevitch LE, Lebedinsky AI. 1957. *On the causes of stellar bursts*. In *Non-stable stars*, ed. GH Herbig, vol. 3 of *IAU Symposium*

Harrington PZ, Garaud P. 2019. *ApJL* 870(1):L5

Hayakawa S. 1955. *Progress of Theoretical Physics* 13(4):464–465

Henkel K, Karakas AI, Lattanzio JC. 2017. *MNRAS* 469(4):4600–4612

Herbig GH. 1963. *AJ* 68:280

Herbig GH. 1965. *ApJ* 141:588

Hobbs LM, Pilachowski C. 1986. *ApJL* 309:L17

Hobbs LM, Pilachowski C. 1988. *ApJ* 334:734

Hobbs LM, Thorburn JA. 1991. *ApJ* 375:116

Hosford A, García Pérez AE, Collet R, Ryan SG, Norris JE, Olive KA. 2010. *A&A* 511:A47

Hurlburt NE, Toomre J, Massaguer JM. 1986. *ApJ* 311:563

Iben Jr. I. 1967. *ApJ* 147:624

Iliadis C, Coc A. 2020. *ApJ* 901(2):127

Imig J, Price C, Holtzman JA, Stone-Martinez A, Majewski SR, et al. 2023. *ApJ* 954(2):124

Izzo L, Della Valle M, Mason E, Matteucci F, Romano D, et al. 2015. *ApJL* 808(1):L14

Jasniewicz G, Parthasarathy M, de Laverny P, Thévenin F. 1999. *A&A* 342:831–838

José J. 2017. *Nucleosynthesis in Novae*. In *14th International Symposium on Nuclei in the Cosmos (NIC2016)*, eds. S Kubono, T Kajino, S Nishimura, T Isobe, S Nagataki, T Shima, Y Takeda

José J, Hernanz M. 1998. *ApJ* 494(2):680–690

José J, Shore SN, Casanova J. 2020. *A&A* 634:A5

Jouve L, Lignières F, Gaurat M. 2020. *A&A* 641:A13

Karakas AI, Lugaro M. 2016. *ApJ* 825(1):26

Kawanomoto S, Kajino T, Aoki W, Bessell M, Suzuki TK, et al. 2009. *ApJ* 701(2):1506–1518

Kawash A, Chomiuk L, Strader J, Sokolovsky KV, Aydi E, et al. 2022. *ApJ* 937(2):64

Kemp AJ, Karakas AI, Casey AR, Côté B, Izzard RG, Osborn Z. 2022a. *ApJL* 933(2):L30

Kemp AJ, Karakas AI, Casey AR, Kobayashi C, Izzard RG. 2022b. *MNRAS* 509(1):1175–1193

King JR, Deliyannis CP, Hiltgen DD, Stephens A, Cunha K, Boesgaard AM. 1997. *AJ* 113:1871

Kiraga M, Rozyczka M, Stepien K, Jahn K, Muthsam H. 2000. *Acta Astronomica* 50:93–104

Knauth DC, Federman SR, Lambert DL. 2003. *ApJ* 586(1):268–285

Knauth DC, Taylor CJ, Ritchey AM, Federman SR, Lambert DL. 2017. *ApJL* 835(1):L16

Korn AJ, Grundahl F, Richard O, Barklem PS, Mashonkina L, et al. 2006. *Nature* 442(7103):657–659

Kos J, Bland-Hawthorn J, Buder S, Nordlander T, Spina L, et al. 2021. *MNRAS* 506(3):4232–4250

Kowkabany J, Ezzeddine R, Charbonnel C, Roederer IU, Wang EX, et al. 2024. *ApJ* 973(2):125

Kraft RP. 1967. *ApJ* 150:551

Kumar P, Quataert EJ. 1997. *ApJL* 475(2):L143–L146

Kumar YB, Reddy BE, Campbell SW, Maben S, Zhao G, Ting YS. 2020. *Nature Astronomy* 4:1059–1063

Kumar YB, Reddy BE, Lambert DL. 2011. *ApJL* 730(1):L12

Lagarde N, Miglio A, Eggenberger P, Morel T, Montalbán J, et al. 2015. *A&A* 580:A141

Lagarde N, Minkevičiūtė R, Drazdauskas A, Tautvaišienė G, Charbonnel C, et al. 2024. *A&A* 684:A70

Lagarde N, Reylé C, Robin AC, Tautvaišienė G, Drazdauskas A, et al. 2019. *A&A* 621:A24

Lagarde N, Romano D, Charbonnel C, Tosi M, Chiappini C, Matteucci F. 2012. *A&A* 542:A62

Lambert DL, Dominy JF, Sivertsen S. 1980. *ApJ* 235:114–125

Lambert DL, Heath JE, Edvardsson B. 1991. *MNRAS* 253:610–610

Le Saux A, Baraffe I, Guillot T, Vlaykov DG, Morison A, et al. 2023. *MNRAS* 522(2):2835–2849

Lèbre A, de Laverny P, de Medeiros JR, Charbonnel C, da Silva L. 1999. *A&A* 345:936–942

Lebreton Y, Goupil MJ, Montalbán J. 2014. *How accurate are stellar ages based on stellar models? II. The impact of asteroseismology*. In *EAS Publications Series*, eds. Y Lebreton, D Valls-Gabaud, C Charbonnel, vol. 65 of *EAS Publications Series*

Lecoanet D, Vasil GM, Fuller J, Cantillo M, Burns KJ. 2017. *MNRAS* 466(2):2181–2193

Lim B, Sung H, Kim JS, Bessell MS, Hwang N, Park BG. 2016. *ApJ* 831(2):116

Lind K, Meléndez J, Asplund M, Collet R, Magic Z. 2013. *A&A* 554:A96

Lind K, Primas F, Charbonnel C, Grundahl F, Asplund M. 2009. *A&A* 503(2):545–557

Liu YJ, Tan KF, Wang L, Zhao G, Sato B, et al. 2014. *ApJ* 785(2):94

Lodders K, Bergemann M, Palme H. 2025. *Sp. Sc. Rev.* 221(2):23

Lu Y, Buck T, Minchev I, Ness MK. 2022. *MNRAS* 515(1):L34–L38

Lu YL, Minchev I, Buck T, Khoperskov S, Steinmetz M, et al. 2024. *MNRAS* 535(1):392–405

Lubin D, Holden BP, Stock C, Melis C, Tytler D. 2024. *AJ* 168(6):240

Maeder A, Meynet G. 2004. *A&A* 422:225–237

Magrini L, Lagarde N, Charbonnel C, Franciosini E, Randich S, et al. 2021. *A&A* 651:A84

Magrini L, Sestito P, Randich S, Galli D. 2009. *A&A* 494(1):95–108

Mallik SV. 1999. *A&A* 352:495–507

Mallik SV, Parthasarathy M, Pati AK. 2003. *A&A* 409:251–261

Marques JP, Goupil MJ, Lebreton Y, Talon S, Palacios A, et al. 2013. *A&A* 549:A74

Martell SL, Shetrone MD. 2013. *MNRAS* 430(1):611–620

Martín E. 2023. *Lithium Across the Universe*

Martos G, Meléndez J, Rathsam A, Carvalho Silva G. 2023. *MNRAS* 522(3):3217–3226

Mathis S. 2009. *A&A* 506(2):811–828

Mathis S. 2025. *A&A* 694:A173

Mathis S, de Brye N. 2011. *A&A* 526:A65

Mathis S, de Brye N. 2012. *A&A* 540:A37

Mathis S, Prat V, Amard L, Charbonnel C, Palacios A, et al. 2018. *A&A* 620:A22

Mathis S, Zahn JP. 2004. *A&A* 425:229–242

Mathur S, García RA, Bugnet L, Santos ÁRG, Santiago N, Beck PG. 2019. *Frontiers in Astronomy and Space Sciences* 6:46

Matsuno T, Aoki W, Beers TC, Lee YS, Honda S. 2017. *AJ* 154(2):52

Matteucci F, D'Antona F, Timmes FX. 1995. *A&A* 303:460

Mazzitelli I, D'Antona F, Ventura P. 1999. *A&A* 348:846–860

McCormick C, Majewski SR, Smith VV, Hayes CR, Cunha K, et al. 2023. *MNRAS* 524(3):4418–4430

McKellar A. 1940. *PASP* 52(310):407

Meduri DG, Jouve L, Lignières F. 2024. *A&A* 683:A12

Meléndez J, Ramírez I, Asplund M, Baumann P. 2010. *Lithium in other Suns: no connection between stars and planets*. In *Light Elements in the Universe*, eds. C Charbonnel, M Tosi, F Primas, C Chiappini, vol. 268 of *IAU Symposium*

Meléndez J, Schirbel L, Monroe TR, Yong D, Ramírez I, Asplund M. 2014. *A&A* 567:L3

Meneguzzi M, Audouze J, Reeves H. 1971. *A&A* 15:337

Meneguzzi M, Reeves H. 1975. *A&A* 40(1-2):99–110

Menn W, Bogomolov EA, Simon M, Vasilyev G, Adriani O, et al. 2018. *ApJ* 862(2):141

Mercer DJ, Austin SM, Brown JA, Danczyk SA, Hirzebruch SE, et al. 2001. *Phys. Rev. C* 63(6):065805

Mestel L, Weiss NO. 1987. *MNRAS* 226:123–135

Michaud G. 1986. *ApJ* 302:650

Michaud G, Alecian G, Richer J. 2015. *Atomic Diffusion in Stars*

Minchev I, Anders F, Recio-Blanco A, Chiappini C, de Laverny P, et al. 2018. *MNRAS* 481(2):1645–1657

Minchev I, Matijevic G, Hogg DW, Guiglion G, Steinmetz M, et al. 2019. *MNRAS* 487(3):3946–3957

Miranda OD. 2025. *arXiv e-prints* :arXiv:2508.09821

Mirouh GM, Baruteau C, Rieutord M, Ballot J. 2016. *Journal of Fluid Mechanics* 800:213–247

Mitler HE. 1970. *SAO Special Report* 330

Molaro P, Bonifacio P, Cupani G, Howk JC. 2024. *A&A* 690:A38

Molaro P, Bonifacio P, Pasquini L. 1997. *MNRAS* 292(1):L1–L4

Molaro P, Izzo L, Bonifacio P, Hernanz M, Selvelli P, della Valle M. 2020. *MNRAS* 492(4):4975–4985

Molaro P, Izzo L, Selvelli P, Bonifacio P, Aydi E, et al. 2023. *MNRAS* 518(2):2614–2626

Molaro P, Primas F, Bonifacio P. 1995. *A&A* 295:L47

Monaco L, Bonifacio P, Sbordone L, Villanova S, Pancino E. 2010. *A&A* 519:L3

Monroe TR, Meléndez J, Ramírez I, Yong D, Bergemann M, et al. 2013. *ApJL* 774(2):L32

Montalbán J. 1994. *A&A* 281(2):421–432

Montalbán J, Schatzman E. 2000. *A&A* 354:943–959

Morel T, Creevey OL, Montalbán J, Miglio A, Willett E. 2021. *A&A* 646:A78

Mosser B, Dréau G, Pinçon C, Deheuvels S, Belkacem K, et al. 2024. *A&A* 681:L20

Mosser B, Goupil MJ, Belkacem K, Michel E, Stello D, et al. 2012. *A&A* 540:A143

Moyano FD, Eggenberger P, Meynet G, Gehan C, Mosser B, et al. 2022. *A&A* 663:A180

Nepal S, Guiglion G, de Jong RS, Valentini M, Chiappini C, et al. 2023. *A&A* 671:A61

Nguyen CT, Cescutti G, Matteucci F, Rizzuti F, Mucciarelli A, et al. 2025. *arXiv e-prints* :arXiv:2508.14594

Nielsen MB, Schunker H, Gizon L, Ball WH. 2015. *A&A* 582:A10

Nordlander T, Gruyters P, Richard O, Korn AJ. 2024. *MNRAS* 527(4):12120–12139

Norris JE, Ryan SG, Stringfellow GS. 1994. *ApJ* 423:386

Norris JE, Yong D, Frebel A, Ryan SG. 2023. *MNRAS* 522(1):1358–1376

Pace G, Castro M, Meléndez J, Théado S, do Nascimento Jr. JD. 2012. *A&A* 541:A150

Palacios A. 2022. *Internal transport processes in stars and the Sun: some updates*. In *The 21st*

*Cambridge Workshop on Cool Stars, Stellar Systems, and the Sun*, Cambridge Workshop on Cool Stars, Stellar Systems, and the Sun

Palacios A, Talon S, Charbonnel C, Forestini M. 2003. *A&A* 399:603–616

Pantillon FP, Talon S, Charbonnel C. 2007. *A&A* 474(1):155–163

Pasquini L, Randich S, Pallavicini R. 2001. *A&A* 374:1017–1029

Pasquini L, Randich S, Zoccali M, Hill V, Charbonnel C, Nordström B. 2004. *A&A* 424:951–963

Peebles PJE. 1966. *ApJ* 146:542

Petitdemange L, Marcotte F, Gissinger C, Daniel F. 2024. *A&A* 681:A75

Piau L, Beers TC, Balsara DS, Sivarani T, Truran JW, Ferguson JW. 2006. *ApJ* 653(1):300–315

Pilachowski C. 1986. *ApJ* 300:289

Pilachowski C, Saha A, Hobbs LM. 1988. *PASP* 100:474

Pitrou C, Coc A, Uzan JP, Vangioni E. 2018. *Phys. Reports* 754:1–66

Planck Collaboration, Aghanim N, Akrami Y, Ashdown M, Aumont J, et al. 2020. *A&A* 641:A6

Prantzos N. 2006. *A&A* 448(2):665–675

Prantzos N. 2010. *PoS* NIC-IX:254

Prantzos N. 2012. *A&A* 542:A67

Prantzos N, Abia C, Chen T, de Laverny P, Recio-Blanco A, et al. 2023. *MNRAS* 523(2):2126–2145

Prantzos N, Casse M, Vangioni-Flam E. 1993. *ApJ* 403:630

Prantzos N, de Laverny P, Guiglion G, Recio-Blanco A, Worley CC. 2017. *A&A* 606:A132

Prat V, Lignières F. 2013. *A&A* 551:L3

Prat V, Mathis S, Augustson K, Lignières F, Ballot J, et al. 2018. *A&A* 615:A106

Press WH. 1981. *ApJ* 245:286–303

Proffitt CR, Michaud G. 1991. *ApJ* 371:584

Ramaty R, Scully ST, Lingenfelter RE, Kozlovsky B. 2000. *ApJ* 534(2):747–756

Ramírez I, Fish JR, Lambert DL, Allende Prieto C. 2012. *ApJ* 756(1):46

Randich S, Aharpour N, Pallavicini R, Prosser CF, Stauffer JR. 1997. *A&A* 323:86–97

Randich S, Pasquini L, Franciosini E, Magrini L, Jackson RJ, et al. 2020. *A&A* 640:L1

Ratcliffe B, Khoperskov S, Minchev I, Lee ND, Buck T, et al. 2024. *arXiv e-prints* :arXiv:2410.17326

Ratcliffe B, Minchev I, Anders F, Khoperskov S, Guiglion G, et al. 2023. *MNRAS* 525(2):2208–2228

Read SM, Viola Jr. VE. 1984. *Atomic Data and Nuclear Data Tables* 31:359

Rebolo R, Molaro P, Beckman JE. 1988. *A&A* 192:192–205

Reeves H. 1993. *A&A* 269(1-2):166–168

Reeves H, Audouze J, Fowler WA, Schramm DN. 1973. *ApJ* 179:909–930

Reeves H, Fowler WA, Hoyle F. 1970. *Nature* 226(5247):727–729

Richard O, Michaud G, Richer J. 2005. *ApJ* 619(1):538–548

Richard O, Michaud G, Richer J, Turcotte S, Turck-Chièze S, VandenBerg DA. 2002. *ApJ* 568(2):979–997

Rogers TM, Glatzmaier GA. 2005. *MNRAS* 364(4):1135–1146

Rogers TM, MacGregor KB. 2010. *MNRAS* 401(1):191–196

Rogers TM, McElwaine JN. 2017. *ApJL* 848(1):L1

Romano D, Magrini L, Randich S, Casali G, Bonifacio P, et al. 2021. *A&A* 653:A72

Romano D, Matteucci F, Molaro P, Bonifacio P. 1999. *A&A* 352:117–128

Romano D, Matteucci F, Ventura P, D’Antona F. 2001. *A&A* 374:646–655

Rüdiger G, Gellert M, Spada F, Tereshin I. 2015. *A&A* 573:A80

Rukeya R, Lü G, Wang Z, Zhu C. 2017. *PASP* 129(977):074201

Ryan SG, Beers TC, Deliyannis CP, Thorburn JA. 1996. *ApJ* 458:543

Ryan SG, Kajino T, Beers TC, Suzuki TK, Romano D, et al. 2001. *ApJ* 549(1):55–71

Ryan SG, Norris JE, Beers TC. 1999. *ApJ* 523(2):654–677

Ryter C, Reeves H, Gradsztajn E, Audouze J. 1970. *A&A* 8:389

Salpeter EE. 1955. *Physical Review* 97(5):1237–1244

Samadi R, Belkacem K, Sonoi T. 2015. *Stellar oscillations - II - The non-adiabatic case*. In *EAS*

Sbordone L, Bonifacio P, Caffau E, Ludwig HG, Behara NT, et al. 2010. *A&A* 522:A26

Scalo JM, Despain KH, Ulrich RK. 1975. *ApJ* 196:805–817

Schatzman E. 1951. *Annales d'Astrophysique* 14:294

Schatzman E. 1993. *A&A* 279(2):431–446

Schwarzschild M, Howard R, Härm R. 1957. *ApJ* 125:233

Sellwood JA, Binney JJ. 2002. *MNRAS* 336(3):785–796

Sengupta S, Garaud P. 2018. *ApJ* 862(2):136

Serenelli A, Weiss A, Aerts C, Angelou GC, Baroch D, et al. 2021. *A&A Review* 29(1):4

Sestito P, Randich S. 2005. *A&A* 442(2):615–627

Shafter AW. 2017. *ApJ* 834(2):196

Shetrone MD, Sneden C, Pilachowski CA. 1993. *PASP* 105:337

Sieverding A, Langanke K, Martínez-Pinedo G, Bollig R, Janka HT, Heger A. 2019. *ApJ* 876(2):151

Simpson JD, Martell SL, Buder S, Bland-Hawthorn J, Casey AR, et al. 2021. *MNRAS* 507(1):43–54

Skoutnev VA, Beloborodov AM. 2025. *ApJ* 988(2):195

Smiljanic R, Franciosini E, Randich S, Magrini L, Bragaglia A, et al. 2016. *A&A* 591:A62

Smiljanic R, Pasquini L, Charbonnel C, Lagarde N. 2010. *A&A* 510:A50

Smith VV, Lambert DL. 1989. *ApJL* 345:L75

Smith VV, Lambert DL. 1990. *ApJL* 361:L69

Smith VV, Plez B, Lambert DL, Lubowich DA. 1995. *ApJ* 441:735

Sneden C, Pilachowski CA. 1986. *ApJ* 301:860

Soderblom DR, Jones BF, Balachandran S, Stauffer JR, Duncan DK, et al. 1993. *AJ* 106:1059

Spada F, Gellert M, Arlt R, Deheuvels S. 2016a. *A&A* 589:A23

Spada F, Gellert M, Arlt R, Deheuvels S. 2016b. *A&A* 589:A23

Spiegel EA, Zahn JP. 1992. *A&A* 265:106–114

Spite M, Francois P, Nissen PE, Spite F. 1996. *A&A* 307:172

Spite M, Spite F. 1982. *Nature* 297(5866):483–485

Spruit HC. 1999. *A&A* 349:189–202

Spruit HC. 2002. *A&A* 381:923–932

Starrfield S, Bose M, Iliadis C, Hix WR, Woodward CE, Wagner RM. 2024. *ApJ* 962(2):191

Starrfield S, Iliadis C, Hix WR. 2016. *PASP* 128(963):051001

Starrfield S, Truran JW, Sparks WM, Arnould M. 1978. *ApJ* 222:600–603

Starrfield S, Truran JW, Sparks WM, Kutter GS. 1972. *ApJ* 176:169

Steigman G, Walker TP. 1992. *ApJL* 385:L13

Steinhauer A, Deliyannis CP. 2004. *ApJL* 614(1):L65–L68

Strugarek A, Belucz B, Brun AS, Dikpati M, Guerrero G. 2023. *Sp. Sc. Rev.* 219(8):87

Sun Q, Deliyannis CP, Anthony-Twarog BJ, Twarog BA, Steinhauer A, King JR. 2025a. *arXiv e-prints* :arXiv:2507.04266

Sun Q, Deliyannis CP, Steinhauer A, Anthony-Twarog BJ, Twarog BA. 2023. *ApJ* 952(1):71

Sun T, Bi S, Chen X, Lu YL, Chen Y, et al. 2025b. *MNRAS* 536(1):462–470

Sun T, Bi S, Chen X, Lu YL, Chen Y, et al. 2025c. *MNRAS* 536(1):462–470

Takeda Y, Honda S, Ohnishi T, Ohkubo M, Hirata R, Sadakane K. 2013. *Pub. of the Astronomical Society of Japan* 65:53

Takeda Y, Kawanomoto S, Honda S, Ando H, Sakurai T. 2007. *A&A* 468(2):663–677

Talon S. 1997. *Hydrodynamique des étoiles en rotation*. Ph.D. thesis, -

Talon S, Charbonnel C. 1998. *A&A* 335:959–968

Talon S, Charbonnel C. 2003. *A&A* 405:1025–1032

Talon S, Charbonnel C. 2004. *A&A* 418:1051–1060

Talon S, Charbonnel C. 2005. *A&A* 440(3):981–994

Talon S, Charbonnel C. 2010. *Light elements as diagnostics on the structure and evolution of low-mass stars*. In *Light Elements in the Universe*, eds. C Charbonnel, M Tosi, F Primas, C Chiappini,

vol. 268 of *IAU Symposium*

Talon S, Kumar P, Zahn JP. 2002. *ApJL* 574(2):L175–L178

Talon S, Richard O, Michaud G. 2006. *ApJ* 645(1):634–651

Talon S, Zahn JP. 1997. *A&A* 317:749–751

Tatischeff V, Raymond JC, Duprat J, Gabici S, Recchia S. 2021. *MNRAS* 508(1):1321–1345

Tayar J, Joyce M. 2022. *ApJL* 935(2):L30

Taylor RJ. 1973. *MNRAS* 161:365

Taylor CJ, Ritchev AM, Federman SR, Lambert DL. 2012. *ApJL* 750(1):L15

Théado S, Vauclair S. 2003. *ApJ* 587(2):795–805

Thorburn JA. 1994. *ApJ* 421:318

Travaglio C, Randich S, Galli D, Lattanzio J, Elliott LM, et al. 2001. *ApJ* 559(2):909–924

Traxler A, Garaud P, Stellmach S. 2011. *ApJL* 728(2):L29

Triana SA, Corsaro E, De Ridder J, Bonanno A, Pérez Hernández F, García RA. 2017. *A&A* 602:A62

Truran JW, Cameron AGW. 1971. *Astroph. & Space Science* 14(1):179–222

Turck-Chièze S, Palacios A, Marques JP, Nghiem PAP. 2010. *ApJ* 715(2):1539–1555

VandenBerg DA, Richard O, Michaud G, Richer J. 2002. *ApJ* 571(1):487–500

Varenne O, Monier R. 1999. *A&A* 351:247–266

Vauclair S. 1988. *ApJ* 335:971

Ventura P, D'Antona F, Mazzitelli I. 2000. *A&A* 363:605–616

Ventura P, Karakas A, Dell'Agli F, García-Hernández DA, Guzman-Ramirez L. 2018. *MNRAS* 475(2):2282–2305

Vrard M, Pinsonneault MH, Elsworth Y, Hon M, Kallinger T, et al. 2025. *A&A* 697:A165

Wachlin FC, Miller Bertolami MM, Althaus LG. 2011. *A&A* 533:A139

Wagoner RV, Fowler WA, Hoyle F. 1967. *ApJ* 148:3

Wallerstein G, Herbig GH, Conti PS. 1965. *ApJ* 141:610

Wallerstein G, Sneden C. 1982. *ApJ* 255:577–584

Wang EX, Nordlander T, Asplund M, Lind K, Zhou Y, Reggiani H. 2022. *MNRAS* 509(1):1521–1535

Wang EX, Nordlander T, Buder S, Ciucă I, Soen A, et al. 2024. *MNRAS* 528(3):5394–5411

Warfield JT, Zinn JC, Schonhut-Stasik J, Johnson JW, Pinsonneault MH, et al. 2024. *AJ* 167(5):208

Weymann R, Sears RL. 1965. *ApJ* 142:174

Wilson OC. 1966. *ApJ* 144:695

Woosley SE, Hartmann DH, Hoffman RD, Haxton WC. 1990. *ApJ* 356:272

Wylie SM, Gerhard OE, Ness MK, Clarke JP, Freeman KC, Bland-Hawthorn J. 2021. *A&A* 653:A143

Young PA, Knierman KA, Rigby JR, Arnett D. 2003. *ApJ* 595(2):1114–1123

Zahn JP. 1992. *A&A* 265:115–132

Zahn JP. 2005. *Processes competing with atomic diffusion: mass loss, turbulence, rotation, etc.* In *EAS Publications Series*, eds. G Alecian, O Richard, S Vauclair, vol. 17 of *EAS Publications Series*

Zahn JP, Talon S, Matias J. 1997. *A&A* 322:320–328

Zappala RR. 1972. *ApJ* 172:57

Zhang H, Chen Y, Zhao G, Bi S, Zhang X, Xue X. 2023. *MNRAS* 520(4):4815–4821

Zhou YT, Shi JR, Yan HL, Gao Q, Zhang JB, et al. 2018. *A&A* 615:A74